Calcareous nannofossil assemblages from El Kef (Tunisia) reveal strong bathymetric controls on Northern Hemisphere recovery patterns following the Cretaceous/Paleogene (K/Pg) mass extinction

Heather L. Jones[1], Lorna Kearns[2], Julio Sepúlveda[3], Chris M. Lowery[4], Laia Alegret[5], Thomas Westerhold[1], M. Hedi Negra[6], Mark Patzkowsky[7] and Timothy J. Bralower[7]

Corresponding author contact: hjones@marum.de

1. MARUM – Center for Marine Environmental Sciences, University of Bremen, Germany.
2. School of Earth and Environment, University of Leeds, UK.
3. Department of Geological Sciences and Institute of Arctic and Alpine Research (INSTAAR), University of Colorado Boulder, USA.
4. Institute for Geophysics, Jackson School of Geosciences, University of Texas at Austin, USA.
5. Departamento de Ciencias de la Tierra & Instituto Universitario de Ciencias Ambientales, Universidad Zaragoza, Spain
6. Faculty of Sciences of Tunis, University of Tunis El Manar, Tunisia
7. Department of Geosciences, Pennsylvania State University, USA

Peer review status: This is a non-peer-reviewed preprint submitted to EarthArXiv.

Calcareous nannofossil assemblages from El Kef (Tunisia) reveal strong bathymetric controls on Northern Hemisphere recovery patterns following the Cretaceous/Paleogene (K/Pg) mass extinction

Heather L. Jones[1], Lorna Kearns[2], Julio Sepúlveda[3], Chris M. Lowery[4], Laia Alegret[5], Thomas Westerhold[1], M. Hedi Negra[6], Mark Patzkowsky[7] and Timothy J. Bralower[7]

Corresponding author contact: hjones@marum.de

8. MARUM – Center for Marine Environmental Sciences, University of Bremen, Germany.
9. School of Earth and Environment, University of Leeds, UK.
10. Department of Geological Sciences and Institute of Arctic and Alpine Research (INSTAAR), University of Colorado Boulder, USA.
11. Institute for Geophysics, Jackson School of Geosciences, University of Texas at Austin, USA.
12. Departamento de Ciencias de la Tierra & Instituto Universitario de Ciencias Ambientales, Universidad Zaragoza, Spain
13. Faculty of Sciences of Tunis, University of Tunis El Manar, Tunisia
14. Department of Geosciences, Pennsylvania State University, USA.

Abstract (250 words)

The Cretaceous/Paleogene (K/Pg) bolide impact ~66 million years ago caused the near-demise of calcareous nannoplankton (coccolithophores): key primary producers and major contributors to the biological pump that exports organic carbon from the surface ocean to the deep sea. Although their mass extinction likely had a profound impact on ecosystem structure and function, the interpretation of early Danian recovery patterns remains challenging due to global heterogeneity in both nannoplankton community dynamics and carbon-cycling responses. To explore this further, we generated a ~3.65 Myr nannofossil record from sediment cores recovered near the classic El Kef (Tunisia) K/Pg boundary section, representing an outer continental shelf/upper slope setting in the peri-Tethys Ocean. Our data revealed four distinct nannoplankton acmes, with transitions between them likely influenced by the progressive restoration of biological pump efficiency. Comparison with previously published datasets from multiple ocean basins and paleoenvironmental settings indicates that the sequence of taxa comprising Northern Hemisphere acme successions were predominantly controlled by paleobathymetry at both a regional and global scale. We speculate that these bathymetric controls on nannoplankton acme characteristics were intrinsically linked to global heterogeneity in the restoration of biological pump efficiency. In particular, nannoplankton acmes marked by extremely small average cell volumes persisted for more than two million years at continental shelf sites, whereas contemporaneous open-ocean sites were dominated by taxa with average cell volumes an order of magnitude larger. Because coccolith calcite enhances organic matter ballasting, we suggest that biological pump efficiency was restored faster in open-ocean settings than in continental shelf environments.

Plain Language Summary

The mass extinction that killed the dinosaurs ~66 million years ago also nearly wiped out calcareous nannoplankton, a group of golden-brown algae that live near the ocean surface. These tiny organisms are important because they provide food for other marine life, and their mineral shells help organic matter sink quickly to the seafloor. Their loss therefore strongly affected marine food webs and the way carbon moves through the ocean. Understanding how nannoplankton recovered after the extinction is difficult because new species appeared and disappeared at different times in different

parts of the world, and the marine carbon cycle also recovered unevenly across regions. To investigate possible connections between nannoplankton recovery and carbon-cycle changes, we studied nannofossils from sediment cores covering about 3.65 million years after the extinction at El Kef in Tunisia. We identified four phases, each dominated by a different nannoplankton species. We think the transitions between these phases were linked to changes in how effectively carbon was transported from the surface ocean to the deep sea. When we compared our record with data from other Northern Hemisphere sites, we found that which species dominated depended strongly on how close the site was to the shore. For example, in deep open-ocean settings, nannoplankton species became larger much earlier than in shallower coastal environments. Because larger shells sink faster and help carry organic matter with them, we suggest that both nannoplankton communities and the carbon cycle recovered sooner in the open ocean than in nearshore regions.

Key Points (Each 140 characters)

- Nannoplankton acmes lasted for more than 3.65 million years after the Cretaceous/Paleogene mass extinction at El Kef.
- A global comparison shows that the specific sequence of nannoplankton taxa that formed acmes was primarily controlled by paleobathymetry.
- Differences in nannoplankton cell size between shelf and open-ocean sites may help explain global variation in biological pump recovery.

1. Introduction

The bolide impact at the Cretaceous/Paleogene (K/Pg) boundary ca. 66 million years ago (Ma) – which most famously wiped out all non-avian dinosaurs (e.g., Alvarez et al., 1980; Chiarenza et al., 2020; Hull et al., 2020; Morgan et al., 2022; Schulte et al., 2010;) – also led to the largest mass extinction in the evolutionary history of calcifying marine plankton (i.e., calcareous nannoplankton and planktonic foraminifera) with >90% species being eliminated (Bown et al., 2004; Fraass et al., 2015; Lowery et al., 2020). In comparison to marine calcifiers, siliceous and organic-walled plankton groups such as diatoms, radiolarians and dinoflagellates, suffered much lower extinction rates, likely due to the ability of some species to form resting cysts (Lowery et al., 2020; MacRae et al., 1996; Sims et al., 2006). Calcareous organisms living at the seafloor (e.g., benthic foraminifera) also did not experience a mass extinction at this time (e.g., Alegret & Thomas, 2013; Alegret et al., 2012, 2022; Culver, 2003; Thomas 1990), underscoring that the K/Pg extinction predominantly affected marine calcifers living in the upper water column (Lowery et al., 2020). This high level of extinction selectivity suggests that short-lived, impact-induced surface ocean acidification may have been an important kill mechanism (Brugger et al., 2021; Henehan et al., 2019) with impact-winter and decreased light availability caused by the emission of dust and aerosols also likely playing a major role (e.g., Brugger et al., 2021; Junium et al., 2022; Morgan et al., 2022; Senel et al., 2023; Vellekoop et al., 2014).

As the most prolific and diverse phytoplankton group at the end of the Cretaceous (Knoll and Follows 2016; Lowery et al., 2020), the near-demise of calcareous nannoplankton at the K/Pg boundary had a major impact on marine ecosystem structure and function. Although primary productivity did not completely cease as originally proposed in the 'Strangelove Ocean' model (Hsü &McKenzie, 1985), vacated niche space in the photic zone was filled by alternative phytoplankton groups including dinoflagellates, diatoms and (especially) cyanobacteria (e.g., Alegret et al., 2022; Bralower et al. 2020; Lowery et al., 2021; Renaudie et al., 2018; Sepúlveda et al., 2019; Vellekoop et al., 2017). The reduced capability of these (predominantly) organic phytoplankton groups to form dense marine aggregates –

especially when compared to the heavily-mineralized, pre-extinction populations of calcareous nannoplankton and planktic foraminifera – severely reduced the effective ballasting of organic carbon from the surface ocean to the seafloor, thus driving decreased biological pump efficiency (i.e., the 'Living Ocean' Model; Alvarez et al., 2019; Birch et al., 2016; Coxall et al., 2006; D'Hondt et al., 1998). However, the mass extinction's effect on biological pump efficiency and export productivity was geographically- and environmentally-variable, as evidenced by site-to-site differences in the magnitude and sign of benthic foraminiferal accumulation rates and diversity, both of which are strongly influenced by the type and amount of food that is transported from the surface ocean to the deep sea (e.g., Alegret & Thomas, 2009, 2013; Alegret et al., 2012, 2022; Hull & Norris, 2011; Sepúlveda et al., 2019;) This so-called 'Hetereogenous Ocean' (Alegret et al., 2022; Esmeray-Senlet et al., 2015; Henehan et al., 2019) was likely a result of taxonomic differences in spatially- and temporally-restricted cyanobacterial blooms, although this has not been thoroughly documented (Alegret et al., 2022; Bralower et al., 2020).

The recovery patterns of calcareous nannoplankton communities during the early Danian were similarly complex. In the Southern Hemisphere, nannoplankton extinction rates were somewhat lower than in the Northern Hemisphere (Jiang et al., 2010) and earliest Paleocene communities consisted of previously-rare survivor taxa that became regionally incumbent for 300 – 400 kyr post-impact (Jiang et al., 2010; Schueth et al., 2015). In contrast, contemporaneous Northern Hemisphere communities were characterized by successive acmes of newly-evolved taxa, which gave rise to the long-ranging lineages that prevailed throughout much of the Paleogene (Alvarez et al., 2019; Bown, 2005; Bown et al., 2023; Jiang et al., 2010, 2019; Jones et al., 2019; Schueth et al., 2015). Although early Danian nannoplankton acmes have been observed at all previously-studied Northern Hemisphere sites, the specific taxa that comprised these successions as well as the duration of the acme 'regime' (Alvarez et al., 2019) were geographically variable (Jones et al., 2019; Schueth et al., 2015). For example, the nannoplankton acme regime ended ca. 1.75 Myr post-impact at Ocean Drilling Program (ODP) Site 1209 (Shatsky Rise) in the pelagic (bathyal) sub-equatorial Pacific Ocean (Alvarez et al., 2019), ca. 2 Myr post-impact at International Ocean Discovery Program (IODP) Site U1407 in the mid-latitude pelagic (abyssal) North Atlantic Ocean (Bown et al., 2023) and ca. 2.5 Myr post-impact at hemipelagic IODP – International Continental Scientific Ocean Drilling (ICDP) Site M0077A in the peak-ring of the Chicxulub impact crater (i.e., at "ground-zero" of the mass extinction event; Jones et al., 2019; Lowery et al., 2021; Figure 1).

There is emerging evidence that the the eventual termination of the nannoplankton acme regime was intrinsically linked to the recovery of biological pump efficiency (Alvarez et al., 2019), which is generally estimated using the surface to deep ocean $\delta^{13}C$ gradient measured on planktic foraminiferal tests (or on bulk sediment) and benthic foraminiferal tests respectively (e.g., Birch et al., 2016, 2021; Coxall et al., 2006; D' Hondt et al., 1998). In the peak ring of the Chicxulub impact crater, the switchovers between nannoplankton acmes are directly coincident with changes in the dominant planktic foraminiferal trophic group, indicating a gradual transition from high-nutrient (eutrophic) to low nutrient (oligotrophic) surface ocean environments that is also consistent with increasing biological pump efficiency (Jones et al., 2019; Lowery et al., 2021). If the recovery of biological pump efficiency – which was globally heterogenous as outlined above (e.g., Alegret et al., 2022; Hull & Norris, 2011) – was strongly coupled to calcareous nannoplankton recovery, it is hardly surprising that there is similarly high geographic variability in the duration and signature of the nannoplankton acme regime. Comparison of nannoplankton acme characteristics between different ocean basins and marine

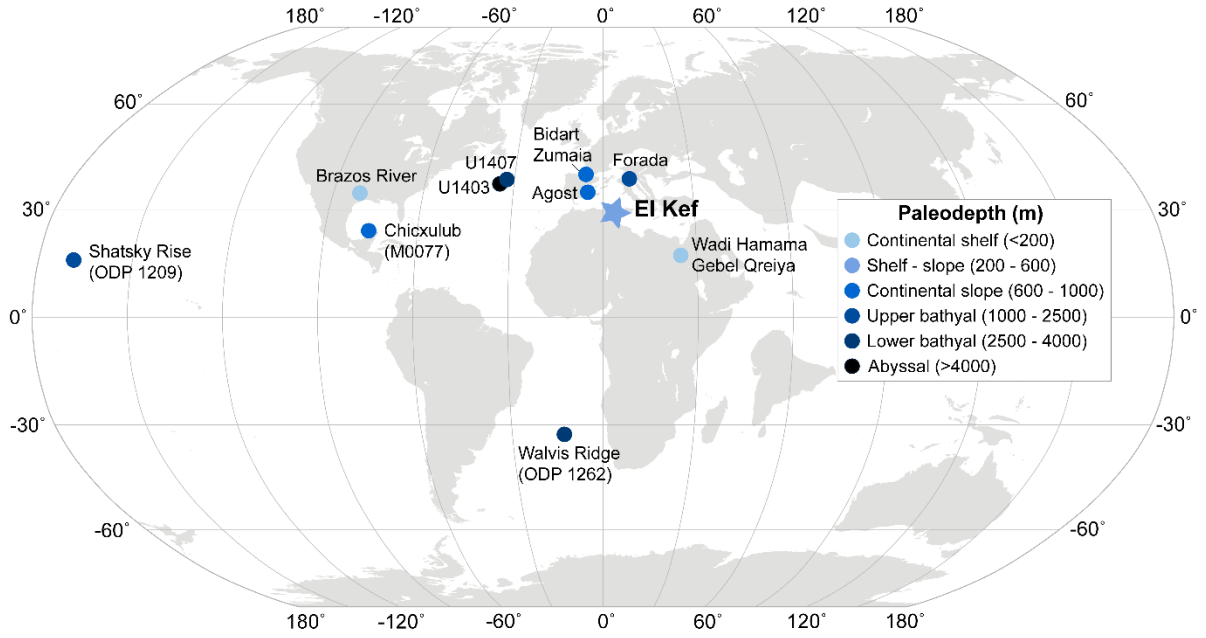

Figure 1. Paleogeographic reconstruction at ~66.0 Ma showing the location of El Kef and other sites discussed in this study. Figure was created using pyGPlates (Mather et al. 2024) using the optimized plate model of Müller et al. (2022).

environments (i.e., continental shelf → abyssal plain), should therefore reveal region- and environment-specific controls on nannoplankton recovery following the largest mass extinction event in their evolutionary history. However, despite having the potential to provide information regarding how organisms at the bottom of the marine food chain respond to rapid episodes of extreme environmental change – which is also important in a modern climate context – such analyses have rarely been conducted (Jiang et al., 2019).

In order to help facilitate these cross-site and cross-environment comparisons, we present here a high-resolution record of Danian calcareous nannofossil assemblages in sediment cores recovered near the Global Stratotype Section and Point (GSSP) for the basal Danian in El Kef (Tunisia). Our new dataset provides one of the longest and most complete nannofossil records from a K/Pg continental shelf site to date, allowing us to:

(a) fully document the nannoplankton acme regime in a shallow marine depositional setting;
(b) compare the nannoplankton acme regime at El Kef to other Tethyan sites, elucidating the potential importance of local processes in ecosystem recovery; and
(c) statistically compare the nannoplankton acme regimes at El Kef and other Northern Hemisphere sites sampling different ocean basins and marine environments, in an attempt to separate out regional and bathymetric controls on acme characteristics (e.g., duration of acmes and the specific acme-forming taxa).

2. Methods

2.1 Study site

During the El Kef Coring Project, sediment cores were recovered from five holes located in close proximity to the GSSP outcrop section, ~5 km southwest of the town of El Kef in northwestern Tunisia (Jones et al., 2023). Due to the drilling process, typical features of the K/Pg boundary observed in the El Kef outcrop (e.g., the 2-3 mm iridium lamina) were not captured in the sediment cores. However,

the integration of biostratigraphic, geochemical and X-Ray Fluorescence (XRF) data led to precise delineation of the boundary and the construction of a composite section ('splice') (Jones et al., 2023). The resultant preferred age model indicates that the Danian was fully and completely recovered in the El Kef cores, apart from a clear unconformity within planktic foraminiferal biozone P1b that was not previously recognized in outcrop. The Danian sediments at El Kef predominantly consist of gray marls (carbonate-rich mudstones) that are darker in color and less heavily bioturbated below the unconformity (Jones et al., 2023). The entire section was deposited at a paleolatitude of 25-30°N in the Tethys Ocean (Figure 1), and samples an outer-shelf to upper-slope paleoenvironment with water depths of 200-600 m (Alegret et al., 2022).

2.2 Age model revision

The current preferred age model for the El Kef cores (Jones et al., 2023) is predominantly based on planktic foraminiferal biostratigraphic datums and is considered to be robust for the early Danian (planktic foraminiferal biozones P0 through the base of P1b). However, reliability of the age model decreases above this due to challenges in identifying biozone markers within the interval immediately above the unconformity in Hole E, which can be attributed to poor preservation, weathering and reworking. There were also some difficulties in precisely delineating the base of the P2 biozone within Hole C as *Praemurica uncinata* (biozone marker for the base of P2) was very rare and had a somewhat spotty occurrence (Jones et al., 2023). Some of the uncertainty with respect to the delineation of the P2 biozone can also be explained – at least in part – by the fact that generally only the 38 – 63 µm size fraction was examined for the biozone marker taxa, thus excluding the larger specimens that became increasingly more common during the Danian.

To further improve the reliability of our age model, planktic foraminiferal biostratigraphy was conducted on the >75 µm size fraction for 28 samples from El Kef Hole C and 44 samples from El Kef E. The specific purpose of these additional analyses was to better constrain the base of P2 and the timing of the unconformity, whilst ensuring biostratigraphic consistency between different size fractions during the earlier Danian (i.e., biozones P0 through P1b). Samples were washed……

2.3 Calcareous nannofossil assemblage counts

Using the El Kef age model and composite section (Jones et al., 2023) as a guide, we chose to use samples from Holes E and C, as combined these represent a nearly stratigraphically continuous K/Pg succession from immediately after the mass extinction event to the base of the *Futyania* acme (planktic foraminiferal biozones P0 to P1c; Hole E), and from the *Futyania* acme to the *Praeprinsius* acme (planktic foraminiferal biozones P1c and P2; Hole C). Nannofossil smear slides were made following the standard procedures outlined in Bown & Young (1998) and examined under cross-polarized light at 1600x magnification. Smear slides were analyzed at a 10 cm sampling resolution between 54.75 and 61.33 meters composite depth (mcd), a 10 to 20 cm sampling resolution between 35.88 and 54.75 mcd and a sampling resolution of 60 cm above this (17.47 – 35.88 mcd). Because the switchovers between K/Pg nannoplankton acmes were geologically rapid events followed by a relatively prolonged interval of quasi-stability, we do not anticipate that the stratigraphic reduction in sampling resolution up-section has drastically altered our results or interpretations. Nannofossil assemblages in the weathered intervals of Holes C and E (above 17.47 mcd and 51.32 mcd respectively) were also examined, but are not included in the subsequent analyses due to clear up-section contamination and poor nannofossil preservation.

At least 300 nannofossil specimens were counted along a random transect in each sample and identified to species-level using the taxonomic concepts of Bown et al. (2023). Replicate counts were also implemented for most samples along a different random transect to improve reliability of the data. Some specimens, including tiny (<2 μm) *Neobiscutum* coccoliths and intermediate, evolutionary morphotypes of all incoming taxa were difficult to identify to species-level, and thus were only assigned a genus. Ultimately, our nannoplankton relative abundance counts resulted in the creation of a large dataset comprising of 186 samples and over 104,000 nannofossil occurrences.

2.4 Statistical analyses

All statistical analyses were conducted on genus-level data, allowing for more reliable comparison of the nannofossil assemblage records compiled by different nannofossil workers whilst still showing meaningful paleoecological trends. Only genera that comprised >2% of an assemblage were included in statistical analyses to limit the formation of outliers that obscure primary paleoecological signals (e.g., Schneider et al. 2013). A Hellinger transformation was then applied to the genus-level assemblage data using the *vegan* package (Oksanen et al.2025) in R (R Core Team, 2025). This transformation first standardizes the data by the sample size (i.e. divides all values in a row by the row sum), which accounts for differences in the total number of specimens counted per sample. It then takes the square root of the values to maximize the importance of rare taxa: vital in teasing apart differences between assemblages that are almost completely dominated by one abundant taxon, as is the case within the early Danian acmes.

2.4.1 Single-site Nonmetric Multidimensional Scaling (NMDS): To statistically analyze the temporal changes in nannofossil assemblages at El Kef, we performed NMDS using the 'metaMDS' function within R's *vegan* package (Oksanen et al.2025; R Core Team 2025). This iterative ordination technique uses a distance measure (in this case the Bray-Curtis distance) to assess the similarity between both samples and species in a dataset. The number of axes (dimensions) used is specific to each data matrix and is manually chosen by the user when the 'stress' value is reduced to a point where it plateaus (in this case 3 dimensions). The resulting ordination plots samples and species as scores on NMDS axes 1 and 2, which explain the greatest amount of variation between samples. We performed three separate NMDS analyses: one using nannoplankton assemblage data from both Holes E and C, one only using assemblage data from Hole E and the last only using data from Hole C. To test whether changes in nannofossil assemblages and paleoenvironmental variables were correlated, we performed a linear regression of the available geochemical data (bulk carbonate $\delta^{13}C$ and $\delta^{18}O$, bulk organic $\delta^{13}C$, % TOC, and % $CaCO_3$; Jones et al., 2023) on the NMDS sample scores using the 'envfit' function in the *vegan* package in R (Oksanen et al.2025; R Core Team 2025). Because geochemical measurements were not always conducted on the same samples as the nannofossil assemblage counts, we linearly interpolated the geochemical values for each of our nannofossil samples. The NMDS and 'envfit' results were then plotted together using the *ggplot2* package (Wickham et al., 2016).

2.4.2 Spearman's Rank correlation plots: Changes in nannofossil assemblages and geochemical proxy data may be decoupled, and only appear to be correlated due to independently-controlled stratigraphic trends. For this reason, the Spearman's rank correlation coefficients between all pairs of columns within a matrix – including relative abundances of the major nannofossil acme taxa, all available geochemical proxy data, and time (in Ma) – were calculated using the 'rcorr' function within

the *Hmisc* package in R (Harrell, 2025; R Core Team 2025). The pairwise correlation matrices were then visualized using the *corrplot* package (Wei & Simko, 2024).

2.4.3 Regional two-way hierarchical cluster analysis: To determine the extent to which regional paleoceanographic conditions played a role in the recovery of calcareous nannoplankton, we performed a two-way cluster analysis using the nannofossil assemblage data from El Kef and six other Tethyan sites from the literature (Fig. 2): Bidart, France (Jiang et al., 2019); Zumaia, Spain (Jiang et al., 2019); Agost, Spain (Jiang et al. 2010); Forada, Italy (Fornaciari et al., 2007); Wadi Hamama, Egypt (Tantawy, 2003) and Gebel Qreiya, Egypt (Tantawy, 2003). Due to the temporal constraints and low-resolution age models of many of the published sites, statistical analyses were restricted to data spanning the first ~3.5 Myr of the Danian. The two-way cluster analysis was performed using the Bray-Curtis distance measure and Ward's linkage method within the *pheatmap* package in R (Kolde 2025). This creates a dendrogram of genera on the x axis and samples on the y axis, with taxa clustering based on co-occurrence among samples, and samples clustering due to similarities in nannofossil assemblage composition.

2.4.4 Northern Hemisphere NMDS: To compare changes in nannofossil assemblages at El Kef to those at other Northern Hemisphere sites, we compiled a dataset using results published in the literature, which sample several different ocean basins and marine environments (Figure 1). In addition to the Tethyan sites listed in Section 2.4.3, five additional sites are included in this Northern Hemisphere dataset: IODP-ICDP Site M0077A in the peak ring of the Chicxulub impact crater, Mexico (Jones et al., 2019); Brazos River, USA (Schueth, 2009); Shatsky Rise (ODP Site 1209), North Pacific Ocean (Alvarez et al., 2019) and IODP Sites U1403 and U1407 in the North Atlantic Ocean (Bown et al., 2023). As in the two-way hierarchical cluster analysis (Section 2.4.3), only data spanning the first ~3.5 Myr of the Danian were used in the NMDS analysis, which was conducted and visualized as an ordination plot using the *vegan* and *ggplot2* packages respectively (Oksanen et al. 2025; Wickham et al., 2016).

3. Results

3.1 Revised El Kef age model

The preservation of planktic foraminifera in the >75 µm size fraction was LORNA/CHRIS PLEASE ADD PRESERVATION STATE HERE. As expected, our revised biostratigraphy shows significant differences in delineation of the two youngest biozones P1c and P2, with additional minor updates to the bases of biozones P1a and P1b (Table 1; Supplementary Table 1; Jones et al. 2023). Delineation of biozones P0 and Pα remains unchanged from the original age model (Jones et al. 2023). Overall, our revised age model suggests that sedimentation rates for biozones P1b and P1c are both lower than originally estimated, with the average for P1b now being ~0.22 cm/kyr (down from 0.33 cm/kyr) and ~0.45 cm/kyr (down from 1.15 cm/kyr) for P1c.

Definitive *Globanomalina compressa* specimens (marker for the base of biozone P1c) and secondary P1c indicators such as *Praemurica inconstans* and *Parasubbotina varianta* were observed within multiple samples at the base of El Kef Hole E Core 4R, 90 to 150 cm, which were not previously examined for planktic foraminiferal biostratigraphy (Jones et al. 2023). These samples are from below the heavily weathered/oxidized depth interval that ranges from the top of Hole E to Hole E Core 4R, ~81 cm (Jones et al. 2023), indicating that the presence of these taxa is likely a primary signal and not a product of downward contamination. These new observations push the depth of base P1c – which was previously placed in a sampling gap between the base of Hole C and top of Hole E Core 5 (~50.63

mcd; Jones et al. 2023) – down to 52.16 mcd (Table 1), which also greatly reduces the error associated with its delineation (from +/- 1.53 m in Jones et al. (2023) to +/- 0.24 m in this study; Supplementary Table 1). Although this improves the reliability of the El Kef age model, it does mean that the unconformity may also include the lowest part of P1c in addition to the upper part of P1b, making it longer than initially estimated (i.e., >500 kyr; Jones et al. 2023). Unfortunately, it is currently unknown exactly how much time is missing from the base of P1c. As only 5 nannofossil samples were counted above the unconformity in Hole E, this uncertainty will not significantly alter our discussion on recovery dynamics, as the remainder of Holes E and C have relatively reliable age control. However, future studies should aim to constrain the length of this unconformity by conducting further stratigraphic work on El Kef Hole D: the only other hole that preserves the actual unconformable contact (Jones et al. 2023).

Biozone	Event	Age (Ma)	Mid-point depth (mcd); Jones et al. 2023	Mid-point depth (mcd); this study
P2	B *Praemurica uncinata*	62.537	34.04	45.64
P1c	B *Globanomalina compressa*	63.978	50.63	52.16
P1b	B *Subbotina triloculinoides*	65.184	54.56	54.76
P1a	T *Parvularugoglobigerina eugubina*	65.690	55.85	55.68
Pα	B *Parvularugoglobigerina eugubina*	66.000	61.06	61.06
P0	B *Guembelitria cretacea*	66.022	61.88	61.88

Table 1. Updated planktic foraminiferal biostratigraphic zonations for the El Kef composite core section compared to the original age model published in Jones et al. (2023). Datums that have undergone major revision are highlighted in orange. Planktic foraminiferal biozones are after Wade et al. (2011) and calibrated to CENOGRID (Westerhold et al. 2020).

The base of P2 was also found to be much lower in this study (~45.64 mcd) than in the initial age model (~34.04 mcd), probably due to increased rarity of the P2 marker taxon *Praemurica uncinata* within the smaller size fraction (38[-63 µm) examined in Jones et al. (2023) compared to the >75 µm size fraction examined here (Table 1). This is supported by the fact that very rare *P. uncinata* specimens were also observed lower in Hole C (~43.75 mcd) within the 38-63 µm size fraction, but were interpreted as downhole contamination due to this taxon's continuous absence within samples from the ~10 m depth interval above this. However, based on our new data from the >75 µm size fraction, the rare *P.uncinata* specimens observed in the 38-63 µm size fraction were actually likely in situ and representative of the smaller forms typical for a species at the beginning of its stratigraphic range. In this case, the exclusion of *P. uncinata* from the 38-63 µm size fraction samples in the overlying 10 m of sediments may be indicative of their rapid evolution to larger average test sizes, with their reappearance in the smaller size fraction at ~34.04 mcd representing their increased relative abundance in assemblages and/or their diversification to encompass a wider range of test sizes.

The marker for the base of planktic foraminiferal zone P3 (*Morozovella angulata*) was not observed in either the 38-63 µm size fraction (examined up to El Kef Hole C 2R, 46-48 cm; Jones et al. 2023) or within the >73 µm size fraction up to the highest examined sample El Kef Hole C 5R, 73-76 cm. Therefore, the entire depth interval between ~14.32 and 45.64 mcd is assigned to biozone P2, which has a duration of ~207,000 years (62.33 to 62.54 Ma). For the purposes of this study, we assume that

14.32 mcd represents the uppermost part of biozone P2 (i.e., 62.33 Ma; the minimum limit), but acknowledge that this depth horizon is potentially much older (but definitely not younger) than this.

3.2 El Kef nannofossil relative abundance data

Overall, the revised El Kef age model indicates that our new nannofossil assemblage data spans the first ~3.67 Myrs of the Danian (Figure 2). Immediately after the K/Pg impact, nannofossils are almost completely absent due to their mass extinction, with assemblages comprising of reworked Cretaceous specimens and the calcareous resting cysts (calcispheres) of dinoflagellates, assigned to *Cervisiella* spp. However, these 'disaster' assemblages only lasted for ~30 kyr, before being replaced by *Neobiscutum*: the first of the incoming Paleocene nannoplankton taxa. *Neobiscutum* immediately dominated assemblages to form a major acme, which persisted for 1.88 Myr (Figure 2a). Within this acme, the

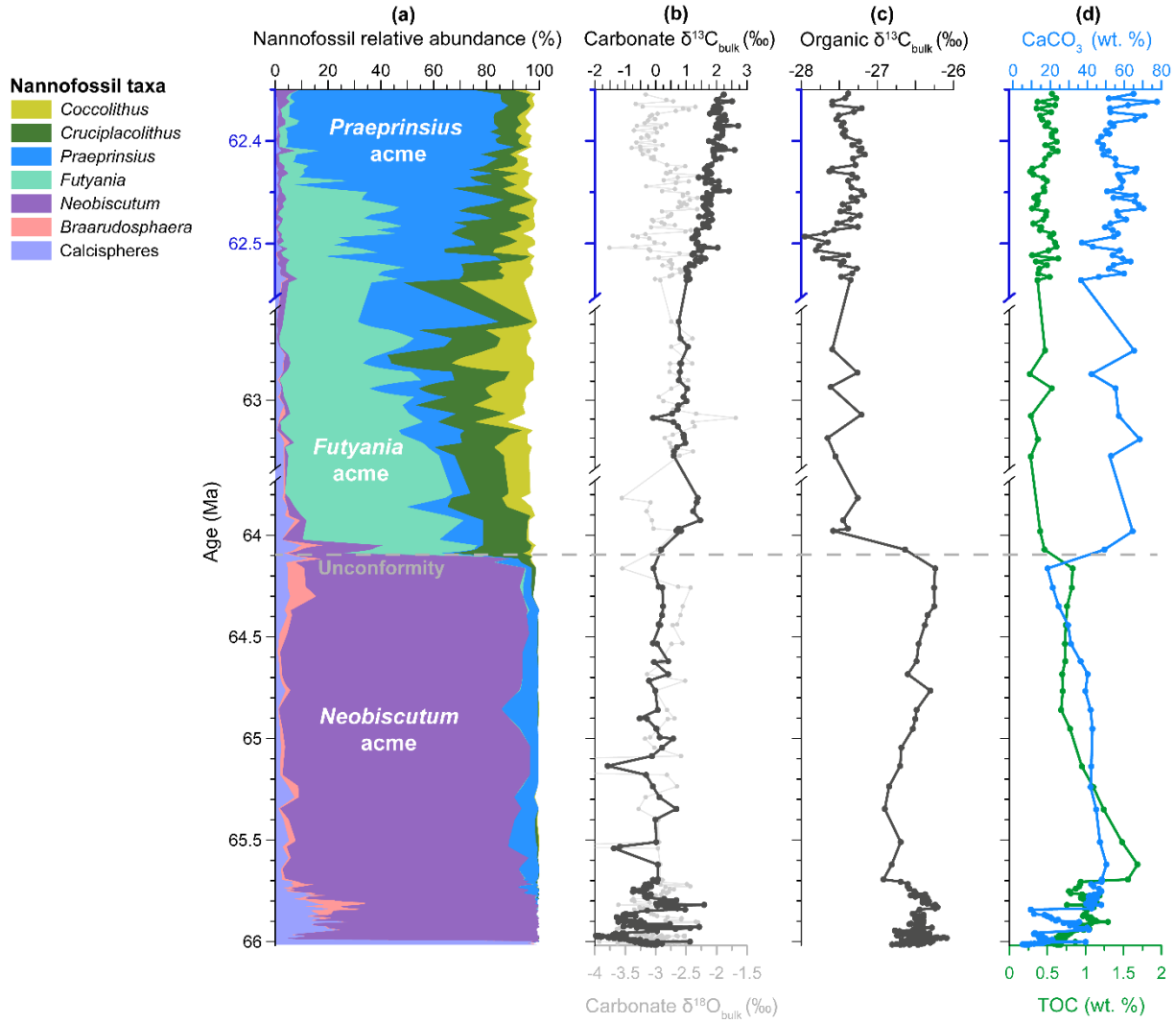

Figure 2. Nannofossil data and geochemical records from ~62.35 – 66.02 Ma in sediment cores from El Kef Tunisia. Please note the two y-axis scale breaks: the first (~63.45 – 63.75 Ma) is a result of the lack of data due to weathering at the top of Hole E, the second (~62.35 – 62.5 Ma) represents a change in scale due to increased sedimentation rates, as highlighted in blue. (a) Cumulative frequency plot showing the relative abundance of the seven most abundant nannofossil taxa. (b) Bulk carbonate $\delta^{13}C$ (black) and $\delta^{18}O$ (light gray) data. (c) Bulk organic $\delta^{13}C$ data. (d) Coulometric data: weight % calcium carbonate ($CaCO_3$; blue) and wt. % Total Organic Carbon (TOC; green).

relative abundance of the nannolith taxon *Braarudosphaera* peaks at ~65.8 Ma, which coincides with an increase in bulk carbonate $\delta^{13}C$ (Figure 2b) and weight percent (%) calcium carbonate ($CaCO_3$; Figure 2d). The subsequent decrease in the relative abundance of *Braarudosphaera* (Figure 2a) is associated with: (a) the continued decline of *Cervisiella* spp; (b) the increased abundance of tiny, ancestral *Praeprinsius* spp. (cf. *vegrandis*; Bown et al. 2023), (c) decreasing trends in both bulk carbonate and bulk organic $\delta^{13}C$ values (Figure 2b; c) and; (d) an overall increase in weight % Total Organic Carbon (TOC; Figure 2d). The remainder of the *Neobiscutum* acme (~64.11 Ma – 65.7 Ma) is characterized by quasi-stable nannofossil assemblages (Figure 2a) and bulk carbonate $\delta^{13}C$ values (Figure 2b), a gradual increase in bulk organic $\delta^{13}C$ (Figure 2c) and a slow decline in both wt. % $CaCO_3$ and TOC (Figure 2d).

At ~64.1 Ma, there is an abrupt transition from the *Neobiscutum* to *Futyania* acme, coinciding with the previously-documented unconformity (Figure 2a). The *Futyania* acme is also associated with the increased relative abundance of long-ranging Paleocene taxa *Cruciplacolithus* and *Coccolithus*, a large increase in bulk carbonate $\delta^{13}C$ (~1.5‰) and wt. % $CaCO_3$ (30%) and a decrease in bulk organic $\delta^{13}C$ and wt. % TOC. The next 1.5 Myr (~62.6 – 64.1) marks an interval of quasi-stability both in terms of nannofossil assemblage composition (Figure 2a) and surface ocean paleoenvironmental conditions as indicated by the stable isotope and coulometric data (Figure 2b-d). Beginning at ca. 62.6 Ma, there was a gradual dominance switchover between *Futyania* and *Praeprinsius*, with a definitive *Praeprinsius* acme becoming fully established by 62.46 Ma. The transition between the *Futyania* and *Praeprinsius* acmes is associated with: (a) a decline in *Cruciplacolithus* and *Coccolithus*, which had previously greatly increased in relative abundance within the *Futyania* acme; (b) a steady ~1.25‰ increase in bulk carbonate $\delta^{13}C$ to the top of the record (~62.35 Ma; Figure 1b); (c) a small, rapid decline in bulk organic $\delta^{13}C$ followed by an increase back to average values; and (d) a sharp decrease from ~65% to 40% weight % $CaCO_3$ at the beginning of the *Futyania* - *Praeprinsius* switchover, followed by highly variable values (35 to 75% wt. % $CaCO_3$) to the top of the examined interval (62.35 to 62.55 Ma; Figure 2d).

3.3 El Kef NMDS and correlation plots

The El Kef NMDS results (Figure 3) confirm the identification of the four distinct acmes observed in the relative abundance data (Figure 2a): (1) the short lived earliest Danian 'disaster' acme, (2) the *Neobiscutum* acme, (3) the *Futyania* acme and, (4) the *Praeprinsius* acme. Overall, the largest change in nannofossil assemblages occurred between the *Neobiscutum* and *Futyania* acmes as indicated by increased sample scores along major NMDS axis 1 (Figure 3a). Changes in assemblage composition between the *Futyania* and *Praeprinsius* acme can be observed as a gradual decrease in NMDS axis 2 sample scores, suggesting a subtler paleoecological transition compared to the *Neobiscutum*→ *Futyania* switchover. The linear regression (environmental fit) of geochemical/coulometric data on the NMDS sample scores shows a statistically significant positive correlation with bulk carbonate $\delta^{13}C$ (r^2=0.7295, p=0.001) and wt. % $CaCO_3$ (r^2=0.5581, p=0.001) and a negative correlation with bulk organic $\delta^{13}C$ (r^2=0.8709, p=0.001) and wt. % TOC (r^2=0.6874, p=0.001), primarily along NMDS axis 1. Subset analyses of the Hole E data (the *Neobiscutum* acme) reinforces these correlations albeit with lower r^2 values (Figure 3b), likely because the sediments within this hole contain the unconformable *Neobiscutum* → *Futyania* transition, which represents the largest paleoecological and paleoenvironmental transition within the entire El Kef record (Figure 3a). In contrast, the separate NMDS analysis for the Hole C samples – which contain the *Futyania* and *Praeprinsius* acmes – only shows a strong, statistically significant correlation with bulk carbonate $\delta^{13}C$ (r^2= 0.664, p=0.001) along

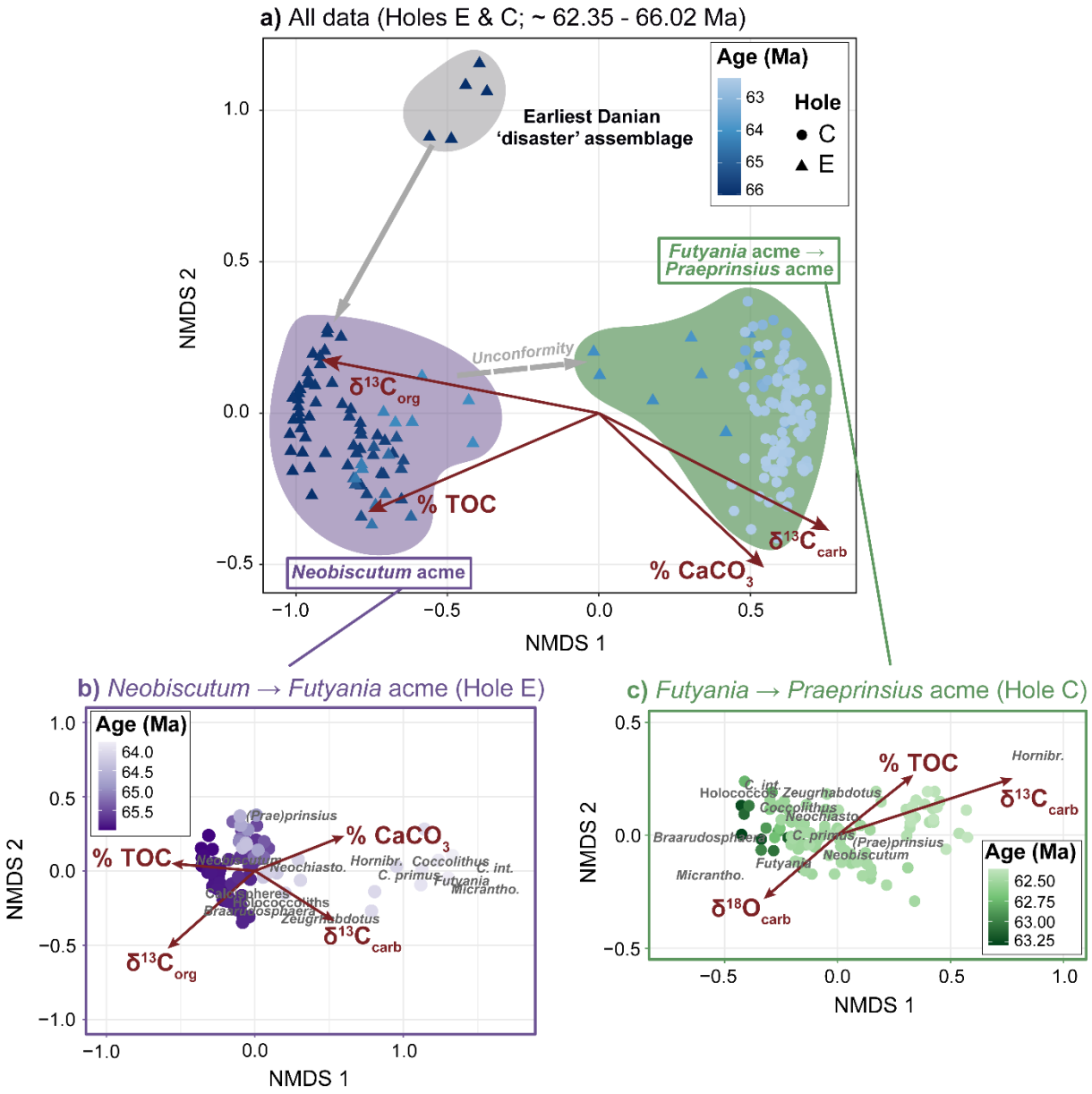

387

Figure 3. Nonmetric multidimensional scaling (NMDS) ordination plots showing the differences between nannofossil assemblages at El Kef. Points (sample scores) that are closer together in ordination space have more similar nannofossil assemblages that those that are further apart. The red vectors on each ordination show the regression ("environmental fit") of the geochemical data on the NMDS scores. The length of each of the vectors correspond to the strength of each of these correlations, with only statistically significant relationships ($p<0.01$) shown. (a) NMDS results for all nannofossil data (~62.35 – 66.02 Ma). (b) NMDS results for the subset of nannofossil data within Hole E, excluding the oldest five samples (~63.79 – 65.99 Ma). (c) NMDS results for the subset of nannofossil data within Hole C (~62.35 – 63.29 Ma).

388 NMDS axis 1 (Figure 3c). Interestingly, the strength of this correlation is higher than in the subset Hole
389 E NMDS results (r^2= 0.4014, p=0.001; Figure 3b).
390
391 Because paleoecological and paleoenvironmental variables may not be directly correlated – and only
392 appear to be due to independent correlation with time – we generated Spearman's rank correlation
393 plots, which show pairwise relationships between multiple variables including estimated ages (Figure
394 4). As expected, the correlation plot using the NMDS axes for the complete El Kef dataset (Figure 3a)

shows that all considered variables are strongly correlated with time (Figure 4a), making it difficult to interpret 'true' correlations between paleoecological and paleoenvironmental variables. The examination of data from the two separate holes using NMDS axes for the complete El Kef dataset (Figure 4b,d) and those from the appropriate subset analyses (Figure 4c, e) show similar results. The one important exception is the apparent negative correlation between the relative abundance of *Neobiscutum* and bulk carbonate $\delta^{13}C$ (Figure 4b, c). In the case of the multi-hole statistical analysis (Figure 4b), NMDS axis 2 does not show a significant statistical correlation with time, but does with both % *Neobiscutum* and bulk carbonate $\delta^{13}C$. This is supported by the single-hole data (Figure 4c), which suggests that changes in the relative abundance of *Neobiscutum* is not significantly correlated to time but is negatively correlated to bulk carbonate $\delta^{13}C$. Although it is important to note that both of these variables are correlated to NMDS 1 axis values – which is itself strongly correlated to time – these results provide tentative evidence that changes in nannofossil assemblages within the *Neobiscutum* acme and during *the Neobiscutum* → *Futyania* switchover were directly linked to increased bulk carbonate $\delta^{13}C$ values. In contrast, the Hole C multi-site data (Figure 4d) shows that

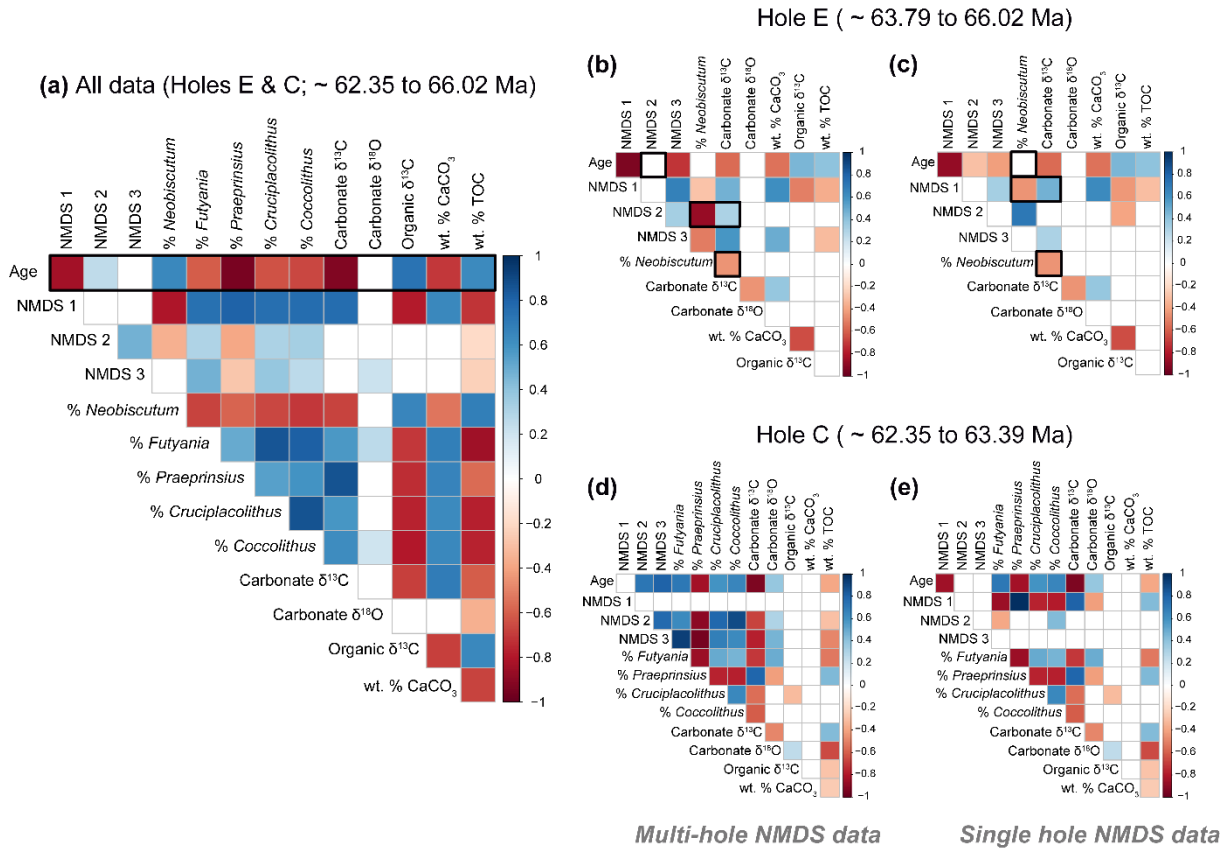

Figure 4. Spearman's rank correlation plots showing the strength of pairwise relationships between multiple variables. Positive relationships ($r^2>0$) are shown in shades of red, whilst negative relationships ($r^2<0$) are shown in shades of blue. Empty boxes (white) represent Spearman's rank correlations with a p value of less than 0.01. (a) Combination of all data from Holes E and C (~62.35 – 66.02 Ma). (b) Subset data from Hole E, with NMDS scores taken from the multi-hole analysis (i.e., Figure 3a; (~63.79 – 65.99 Ma)). (c) Subset data from Hole E, with NMDS scores taken from the Hole E single-hole analysis (i.e., Figure 3b; (~63.79 – 65.99 Ma)). (d) Subset data from Hole C, with NMDS scores taken from the multi-hole analysis (i.e., Figure 3a; (~62.35 – 63.29 Ma)). (e) Subset data from Hole C, with NMDS scores taken from the Hole C single-hole analysis (i.e., Figure 3c; (~62.35 – 63.29 Ma)).

NDMS 1 is not significantly correlated to any of the variables, including time. Instead time is correlated with NMDS axis 2 – and even more so with NMDS axis 3 – which are both in turn correlated with most other considered paleoecological and paleoenvironmental parameters (excluding bulk organic $\delta^{13}C$ and wt. % $CaCO_3$). Although the single hole-analysis for Hole C indicates that time is not significantly correlated to NMDS axes 2 and 3 (Figure 4e), the relative abundance of *Futyania* and *Coccolithus* are the only variables that are significantly correlated with either of these axes. Therefore, it is not possible to make the same speculative link between changes in nannofossil assemblages and bulk carbonate $\delta^{13}C$ within the *Futyania* and *Praeprinsius* acmes as in the earlier *Neobiscutum* acme.

3.4 Regional cluster analysis

The two-way hierarchical cluster analysis conducted on our new El Kef data and additional published records from a range of other Tethyan sites, reveals three major clusters related to distinct nannofossil acmes (Figure 5). Cluster 1 comprises of 3 sub-clusters and represents the earliest Danian 'disaster' acme. Sub-cluster 1A-I is characterized by the almost complete dominance of calcispheres within samples from Wadi Hamama and Gebel Qreiya, as well as the oldest 5 samples from El Kef. Calcispheres also dominate the sub-cluster 1A-II samples, but can be distinguished from sub-cluster 1A-I by the relatively high abundance of Cretaceous survivor taxon *Cyclagelosphaera*. Samples from sub-cluster 1A-II are predominantly from Bidart and Zumaia, with one sample from Forada. Sub-cluster 1B is characterized by a calcisphere acme with relatively high abundances of *Neobiscutum* and low holococcolith abundance (1B-I) or with a high relative abundance of *Braarudosphaera* (1B-II). Samples from the former are restricted to the Egyptian continental shelf sites Wadi Hamama and Gebel Qrieya, whilst the latter predominantly comprises of samples from Forada and Zumaia. The last sub-cluster within cluster 1 consists of a *Braarudosphaera* acme with relatively high abundances of *Neobiscutum* and low abundances of calcispheres (samples from Zumaia, Agost, Wadi Hamama and Gebel Qrieya; sub-cluster 1C-I) or a *Braarudosphaera* acme with relatively high abundances of *Cyclagelosphaera,* calcispheres, and/or holococcoliths and low abundances of *Neobiscutum* (samples from Bidart, Agost and Forada; sub-cluster 1C-II). Samples from El Kef are completely absent from sub-clusters 1B and 1C.

Cluster 2 represents the *Neobiscutum* acme and almost entirely consists of samples from El Kef (Figure 5). Subcluster 2A is characterized by the very high abundance of *Neobiscutum* with a lower abundance of calcispheres (2A-I) or early *Praeprinsius* cf. *vegrandis* (2A-II). In comparison, samples within Subcluster 2B have slightly lower relative abundances of *Neobiscutum* with a higher proportion of calcispheres (2B-I) or with increased relative abundances of calcispheres, holococcoliths and *Braarudosphaera* (2B-II). Sub-cluster 2B-II is the only group to contain samples that are not from El Kef (Agost and Bidart).

The last major cluster (Cluster 3) contains samples from the latest part of the K/Pg recovery interval included in this analysis. Sub-cluster 3A represents the *Praeprinsius* acme at Forada, which also features lower abundances of *Coccolithus* and *Cruciplacolithus*. In contrast, sub-cluster 3B – which only comprises samples from El Kef – is characterized by the *Futyania* acme, with relatively high abundances of *Cruciplacolithus*, variable abundances of *Praeprinsius* and either a very low (3B-I) or relatively high (3B-II) proportion of *Coccolithus*. Sub-cluster 3C predominantly consists of samples from Forada, and is representative of a *Coccolithus* acme with a relatively high proportion of *Cruciplacolithus* and either a low (3C-I) or relatively high (3C-II) abundance of *Praeprinsius*. The last sub-cluster (3D) only contains samples from Zumaia, and is characterized by a *Coccolithus* acme with a relatively high abundance of

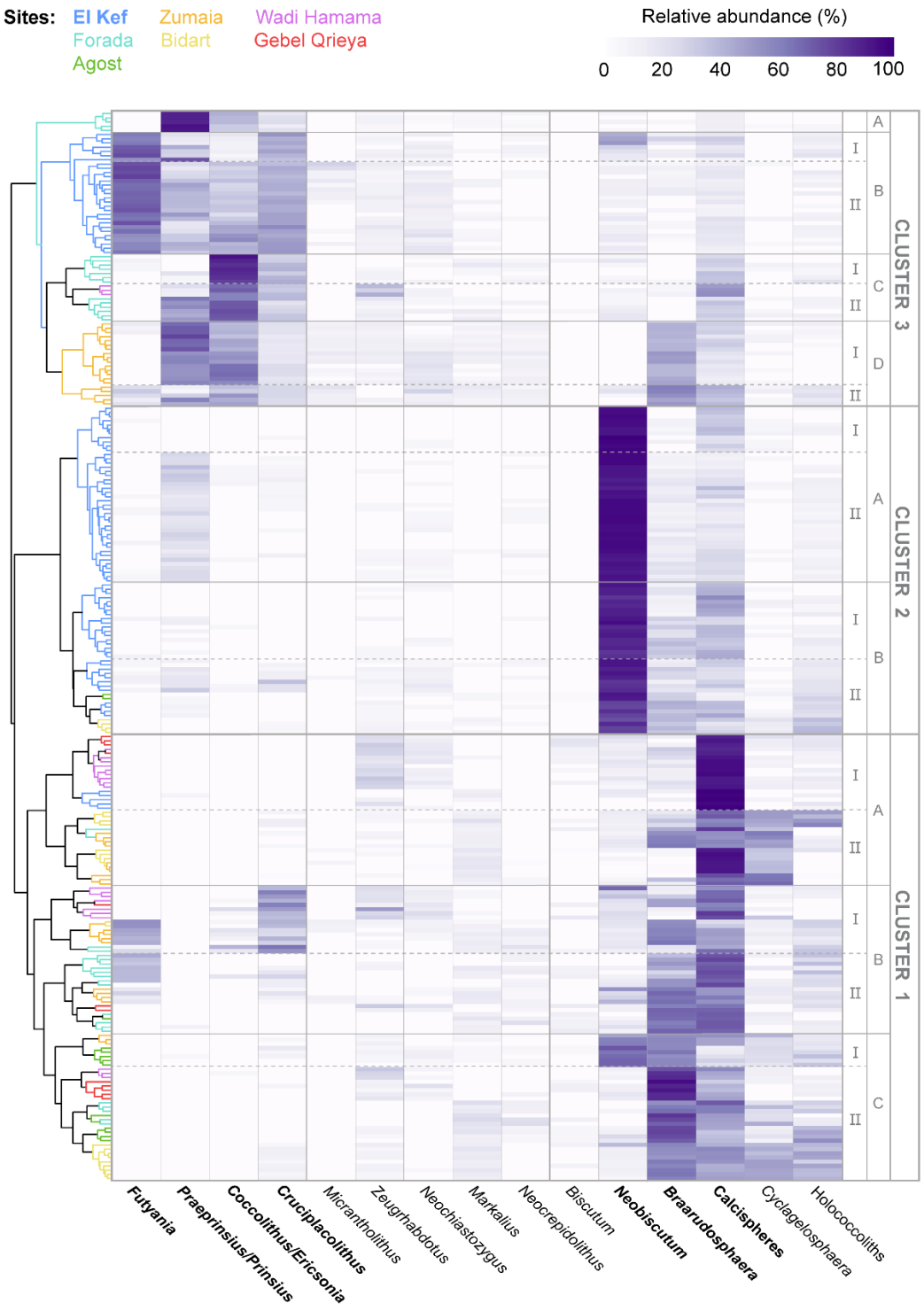

454

Figure 5. Dendrogram showing the results of a regional (Tethyan) two-way cluster analysis or 'heatmap' conducted on nannofossil relative abundance data. The horizontal (x-axis) dendrogram shows the clustering of nannofossil genera and the vertical (y-axis dendrogram) shows clustering between samples, with the site that the sample is from distinguished by color: blue = El Kef (this study), teal = Forada (Fornaciari et al. 2007), green = Agost (Jiang et al. 2010), orange = Zumaia (Jiang et al. 2019), yellow = Bidart (Jiang et al. 2019), pink = Wadi Hamama (Tantawy 2003) and red = Gebel Qrieya (Tantawy 2003). The relative abundances of nannofossil taxa are also shown in accordance with the scalebar to the top-right of the figure.

Braarudosphaera and either a higher proportion of *Praeprinsus* (3D-I) or comparatively higher relative abundances of calcispheres, holococcoliths and *Futyania* (3D-II).

3.5 Northern Hemisphere NMDS analysis

To compare Tethyan nannoplankton recovery patterns for the first ~3.5 Myr of the Danian to those in other Northern Hemisphere ocean basins, we conducted a further NMDS analysis with sample scores coded by both location (site and region; Figure 6a) and estimated paleobathymetry (Figure 6b). Our results reveal that the largest change in nannofossil assemblages – as observed along NMDS axis 1 – are associated with the transition from post-extinction acmes (high NMDS axis 1 scores) to the formation of more diverse communities (low NMDS axis 1 scores). However, it is important to note that within the examined 3.5 Myr time frame, only three open ocean sites – ODP Site 1209 (Shatsky Rise, subtropical Pacific Ocean) and IODP Sites U1403 & U1407 (mid-latitude North Atlantic Ocean) – completed the full transition to stable nannofossil assemblages comprising of long-ranging Paleocene taxa such as *Cruciplacolithus*, *Coccolithus*, *Toweius* and *Fasciculithus*.

The two major pathways leading to the establishment of stable assemblages is dependent on the immediate post-impact community composition (Figure 6a). For almost all of the Tethyan sites and IODP-ICDP Site 364 (Chicxulub impact crater, Gulf of Mexico), early nannofossil assemblages consist of relatively high abundances of calcispheres, *Braarudosphaera* and/or *Cyclagelosphaera,* with a stratigraphic transition to increased *Cruciplacolithus* and/or *Coccolithus* abundances. Alternatively,

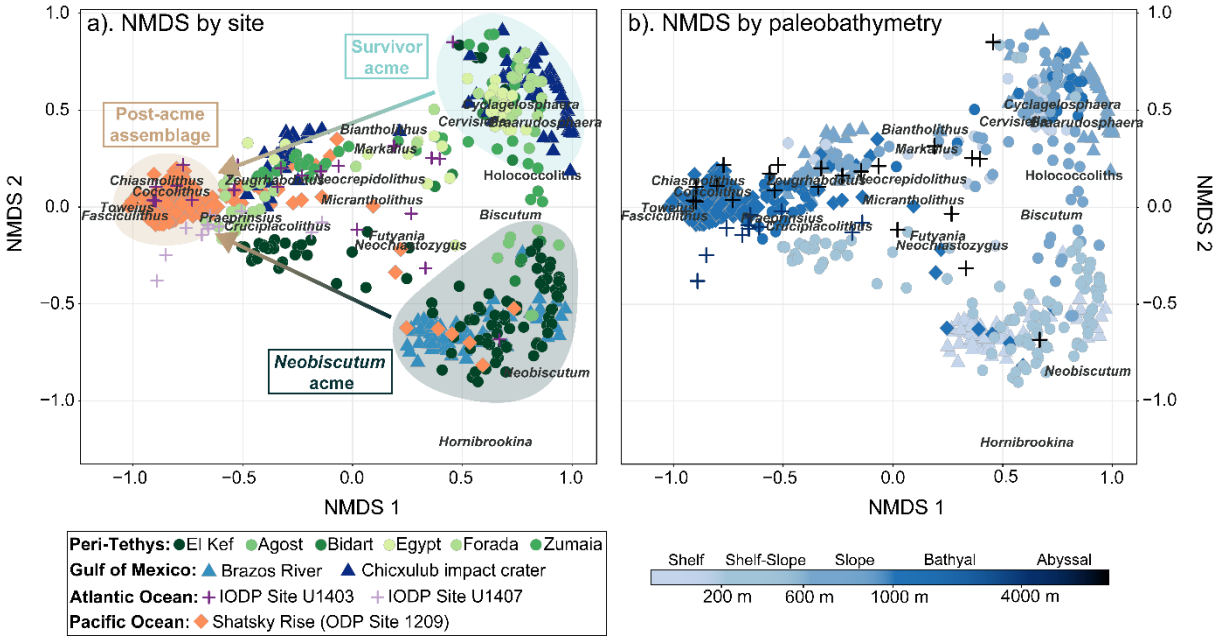

Figure 6. Nonmetric multidimensional scaling (NMDS) ordination plot for the global literature data. (a) Sample scores coded by region (shape) and site (color). Sites from the peri Tethys Ocean (circles) are El Kef (this study), Agost (Jiang et al. 2010), Bidart (Jiang et al. 2019), Egypt (Wadi Hamama & Gebel Qrieya; Tantawy 2003), Forada (Fornaciari et al. 2007) and Zumaia (Jiang et al. 2019). Sites from the Gulf of Mexico (triangles) are Brazos River (Schueth 2009) and IODP-ICDP Site M0077A: Chicxulub impact crater (Jones et al. 2019). Sites from the North Atlantic Ocean (crosses) are IODP Site U1403 and IODP Site U1407 (Bown et al. 2023). Site from the North Pacific Ocean (diamonds) is ODP Site 1209: Shatsky Rise (Alvarez et al. 2019). (b) Sample scores coded by paleobathymetry.

earliest Danian assemblages from El Kef, Brazos River (USA), ODP Site 1209 and IODP Site 1403 are characterized by a well-defined *Neobiscutum* acme. Although a few samples from Bidart and Agost also show an increased relative abundance of *Neobiscutum* during the recovery interval, this taxon does not form a true acme as at the aforementioned four sites. The short-lived *Neobiscutum* acme at both ODP Site 1209 and IODP Site U1403 is followed by a succession of dominance switchovers (*Cruciplacolithus* → *Praeprinsius* → *Coccolithus*) prior to the establishment of more permanent, stable Paleocene assemblages. In contrast, at El Kef, the *Neobiscutum* acme is succeeded by the *Futyania* acme (which is also characterized by an increased abundance of *Cruciplacolithus*), whilst assemblages at Brazos River remain within the *Neobiscutum* acme for the entire examined time interval.

4. Discussion

4.1 Calcareous nannoplankton recovery dynamics at El Kef

The raw nannofossil relative abundance data (Figure 2a) and NMDS results (Figure 3) reveal the existence of four distinct acmes at El Kef, with the switchovers between them marking major milestones in the nannoplankton recovery. Below we discuss the nannofossil assemblage data and geochemical records for each of these acmes in turn, providing clues as to the potential paleoenvironmental and/or paleoecological conditions during each recovery stage.

4.1.1 Stage 1 – The earliest Danian 'disaster' assemblage (~66.00 to 66.02 Ma): The oldest five samples examined in the El Kef cores – which represent the first ~20 kyr of the Danian – contain only *Cervisiella* calcispheres (calcareous cysts produced by dinoflagellates) and reworked late Cretaceous nannofossil species such as *Watznaueria barnesiae*, *Micula* spp. and *Prediscosphaera* spp. This calcisphere "spike" is a global feature driven by the near-total extinction of calcareous nannoplankton (e.g., Lamolda et al., 2016; McLachlan & Pospelova, 2021; Romein, 1977), which opened up niche space that was subsequently filled by plankton groups less severely affected by the K/Pg impact (e.g., Sepúlveda et al., 2019). In addition to calcareous dinoflagellates, this included presumed opportunistic, heterotrophic organic-walled dinoflagellate taxa (Vellekoop et al., 2015) and cyanobacteria (Bralower et al., 2020; Sepúlveda et al., 2019), all of which have resting stages that allowed them to wait out the extreme environmental conditions (e.g., global darkness and impact winter) that persisted for the decades to centuries following the bolide impact. Although these environmental effects were geologically short-lived, an increasing body of evidence suggests prolonged surface ocean instability, potentially driven by: (1) pH overshoot following a transient ocean acidification event (up to ~40 kyr post-impact; Henehan et al., 2019), (2) long-term (~100 kyr) global warming due to increased atmospheric CO_2 from wildfires, soil decay and/or impacted target rock (Artemieva et al., 2017; Macleod et al., 2025; Morgan et al., 2022) and/or, (3) increased upwelling due to cooling-induced vertical mixing, leading to surface ocean nutrient enrichment (eutrophication) for up to 1000 years post-impact (Brugger et al., 2016). Such environmental instability is supported by major variability in bulk organic $\delta^{13}C$ values (-26.80 to -26.27 ‰) during the first 20 kyr of the Danian at El Kef, which could reflect fluctuations in terrestrial- vs. marine-derived organic material, changes in non-calcifying phytoplankton community composition, or changes in the isotopic fractionation of carbon during photosynthesis due to the aforementioned increase in atmospheric CO_2. Although not possible with our current bulk organic geochemical data, upcoming high-resolution, compound-specific $\delta^{13}C$ records from El Kef will be able to determine which of these options was most likely.

In contrast to the bulk organic $\delta^{13}C$ data, bulk carbonate $\delta^{13}C$ values show a general ~-0.7 ‰ decrease during the same interval. This was likely driven by the mass extinction of almost all latest Maastrichtian nannoplankton and planktic foraminifera species, which have relatively high $\delta^{13}C$ signatures compared to the calcareous dinoflagellates and small, non-symbiotic planktonic foraminifera that replaced them (e.g., Alegret et al., 2012, 2022; Birch et al., 2016; Esmeray-Senlet et al., 2015; Sepúlveda et al., 2019). In addition, the absence of relatively dense, heavily calcified calcareous nannoplankton and planktic foraminifera taxa from earliest Danian communities, meant that organic matter was not transported from the surface ocean to the deep sea as effectively as it was during the latest Maastrichtian. This reduction in biological pump efficiency led to increased remineralization in the surface ocean, driving down the $\delta^{13}C$ value of the planktic organisms that comprise the majority of bulk carbonate in deep-sea sediments (Figure 7a; Birch et al., 2016; D'Hondt et al., 1998; Henehan et al., 2019). Therefore, the decrease in bulk carbonate $\delta^{13}C$ likely represents the joint effect of the increased dominance of ^{13}C-depleted plankton taxa in surface ocean communities and reduced biological pump efficiency. However, it could also at least partially be explained by the increased abundance of non-biogenic carbonate – including diagenetic dolomite crystals – which are commonly observed in smear slides from both the El Kef sediment cores (this study) and outcrop section (Sepúlveda et al., 2019).

4.1.2 Stage 2 – The *Neobiscutum* acme (~64.11 to 66.00 Ma): Approximately 20 kyr after the mass extinction event, the earliest Danian disaster assemblages at El Kef were replaced by the *Neobiscutum* acme. This tiny, lightly calcified genus produced coccoliths <2 µm in length and likely evolved immediately after the K/Pg impact (Bown, 2005; Bown et al., 2023; Jiang et al., 2019) or during the

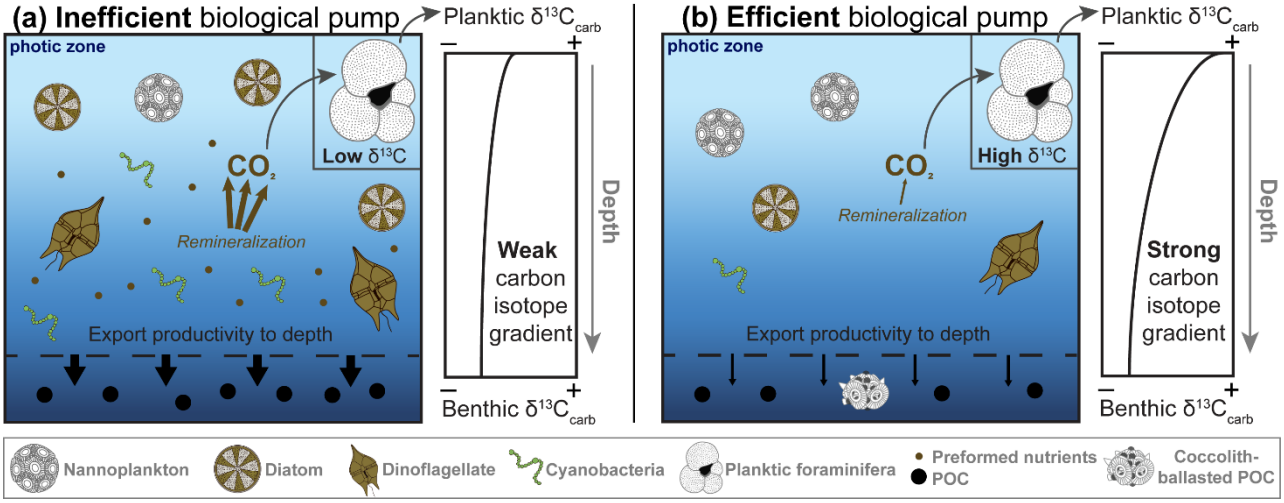

Figure 7. Conceptual model of an inefficient (a) versus efficient (b) biological pump. (a) An inefficient biological pump arises due to incomplete nutrient utilization by phytoplankton, with only a small fraction converted to organic matter and exported to the deep sea. This results in nutrient-rich (eutrophic) surface waters that favors plankton groups such as cyanobacteria and dinoflagellates and opportunistic, generalist nannoplankton taxa (e.g., *Neobiscutum*) or those well-adapted to eutrophic environments (e.g., *Braarudosphaera*). Increased remineralization in the upper water column leads to reduced planktic foraminiferal $\delta^{13}C$ and a weak carbon isotope gradient. (b) An efficient biological pump arises when nutrients are fully utilized by phytoplankton, converted into organic matter and exported to the deep sea. This depletes surface nutrients, favoring low-nutrient (oligotrophic)-adapted groups such nannoplankton, especially 'typical' specialized taxa (e.g., *Cruciplacolithus* and *Coccolithus*). Relatively low surface ocean remineralization results in higher planktic foraminiferal $\delta^{13}C$ and a strong carbon isotope gradient.

latest Maastrichtian (Mai et al., 2003; Schueth et al., 2015). *Neobiscutum* is morphologically similar to the dominant nannoplankton species in the modern ocean – *Gephyrocapsa* (formerly *Emiliania*) *huxleyi* – and is widely considered to have been an opportunistic, generalist taxon that was able to take advantage of high nutrient (eutrophic) surface ocean environments (e.g., Bown, 2005; Jiang et al., 2010; Jiang et al., 2019). Such conditions likely prevailed at El Kef due to reduced biological pump efficiency and increased remineralization within the ocean mixed layer, explaining the exceptionally high dominance of *Neobiscutum* (60-95% of assemblages) at this outer shelf/upper slope site (Figures 2a; 5; 6).

Beginning at approximately ~65.85 Ma, there was an increase in the relative abundance of both calcispheres and *Braarudosphaera* (Figure 2a), the latter of which reaches a maximum of 20% at 65.81 Ma. Interestingly, this paleoecological shift roughly coincides with a transient ~1 ‰ decrease in bulk carbonate $\delta^{18}O$ between ca. 65.90 and 65.82 Ma (Figure 2b), suggesting a brief interval of surface ocean warming. Although the bulk carbonate $\delta^{18}O$ record should be interpreted with caution due to its low signal to noise ratio, changes in other geochemical parameters are also apparent including: (1) a ~2 ‰ decrease in bulk carbonate $\delta^{13}C$ between 65.93 and 65.86 Ma (Figure 2b) followed by a return to pre-excursion values between 65.86 and 65.82 Ma (2) a decrease in carbonate content from 40 to 10 wt. % between 65.94 and 65.84 Ma (Figure 2d) and, (3) a ~0.5% decrease in wt. % TOC between 65.90 and 65.82 Ma (Figure 2d). These geochemical signatures closely resemble those of the astronomically-paced Dan-C2 hyperthermal event, which occurred ~160 kyr after the K/Pg boundary (i.e., ca. 65.86 Ma) and has been recognized at various Atlantic and Tethyan sites (e.g., Arreguín-Rodríguez et al., 2021; Barnet et al., 2019; Coccioni et al., 2010). Notably, at Gubbio (Italy), a *Braarudosphaera* spike is coincident with the onset of the Dan-C2 event (Coccioni et al., 2010), supporting the identification of this earliest Paleogene hyperthermal within the El Kef sediment cores. Similar to *Neobiscutum*, the extant Cretaceous survivor *Braarudosphaera* is adapted to high nutrient environments, being restricted to coastal regions in the modern ocean (e.g., Hagino et al., 2009; Takano et al., 2006). As *Neobiscutum* remains the dominant component of nannofossil assemblages during the Dan-C2 event, it is unlikely that changes in nutrient availability were the direct cause of the *Braarudosphaera* spike. Instead, we suggest that Dan-C2 warming led to hyperstratification of the upper water column, leading to temporarily reduced surface water salinity: a mechanism proposed for the formation of astronomically-paced *Braarudosphaera* acmes in the mid-Oligocene South Atlantic Ocean (Liebrand et al., 2018).

The decreased relative abundance of *Braarudosphaera* after the Dan-C2 event marks a return to almost monospecific *Neobiscutum* assemblages, albeit with a small, sustained increase in ancestral *Praeprinsius* (cf. *vegrandis*). From ~65.76 Ma to the top of the *Neobiscutum* acme (~64.11 Ma) nannofossil assemblages remain relatively stable (Figure 2a). This interval is also associated with a gradual decline in wt. % $CaCO_3$ (following a prior sharp increase, likely driven by the increased abundance of heavily-calcified *Braarudosphaera*), a gradual ~0.75 ‰ increase in bulk organic $\delta^{13}C$ and a sharp decrease in wt. % TOC followed by a steady decrease to the top of the *Neobiscutum* acme (Figure 2c, d). In contrast, there is very little change in the bulk carbonate $\delta^{18}O$ or $\delta^{13}C$ records (Figure 2b), the latter of which fluctuates around an average value of -0.07 ‰. Although the planktic-to-benthic foraminiferal $\delta^{13}C$ gradient (Figure 7) would ideally be used to evaluate changes in biological pump efficiency during the *Neobiscutum* interval, these data are not yet available for the El Kef cores. However, a previous study at Walvis Ridge in the mid-latitude South Atlantic suggests that the

585 increased vertical $\delta^{13}C$ gradient during the early Danian was predominantly driven by increased
586 planktic foraminiferal $\delta^{13}C$ rather than decreased benthic foraminiferal $\delta^{13}C$ (Birch et al., 2016).
587 Assuming that this is the case, the relatively static bulk carbonate $\delta^{13}C$ values indicates continued
588 inefficient carbon cycling at El Kef for at least 1.9 Myr post-impact, which is supported by the negative
589 correlation between the relative abundance of *Neobiscutum* and bulk carbonate $\delta^{13}C$ (Figure 4).
590 Biological pump inefficiency was likely driven – at least in part – by the dominance of *Neobiscutum*,
591 which had an average cell volume an order of magnitude smaller than the later, long-ranging
592 Paleocene taxa (Alvarez et al., 2019). This would have severely reduced the effectiveness of coccolith
593 calcite in ballasting organic matter, thus maintaining biological pump inefficiency and high-nutrient
594 surface oceans that further bolstered the *Neobiscutum* acme. Therefore, it is likely that the restoration
595 of biological efficiency at El Kef could not begin properly until *Neobiscutum* was displaced.
596
597 **4.1.3 Stage 3 – The *Futyania* acme (~62.46 to 64.11 Ma):** The switchover between the *Neobiscutum*
598 and *Futyania* acmes occurs across the ~64.11 Ma unconformity (Figures 2a; 3a) and is associated with:
599 (1) a ~1.5 ‰ increase in bulk carbonate $\delta^{13}C$ (Figure 2b), (2) a ~1 ‰ decrease in bulk organic $\delta^{13}C$
600 (Figure 2c) and, (3) a tripling of wt. % $CaCO_3$ (Figure 2d). As the duration of the unconformity is currently
601 poorly constrained, it is not possible to ascertain how quickly this paleoecological transition occurred.
602 However, the large changes observed in almost all of our geochemical records signal a major regime
603 shift (Figure 3b), with ecosystem function being very different compared to that within the preceding
604 *Neobiscutum* acme. In particular, the concurrent increase in bulk carbonate $\delta^{13}C$ and decrease in bulk
605 organic $\delta^{13}C$, suggests that the *Neobiscutum* → *Futyania* dominance switchover marks the first
606 milestone in the restoration of biological pump efficiency (Figure 7). This meant that a higher
607 proportion of the nutrients in the surface ocean were utilized by phytoplankton, converted into organic
608 matter and exported to the deep sea, lowering mixed layer remineralization and reducing nutrient
609 availability. Lower nutrient (meso/oligotrophic) conditions would have favored the proliferation of
610 typical open-ocean taxa such as *Cruciplacolithus*, as supported by their increased relative abundance
611 in line with the onset of the *Futyania* acme at El Kef (Figure 2b). Although the paleoecological
612 preferences of *Futyania* itself are uncertain, it is likely that it was better-adapted to lower nutrient
613 conditions than *Neobiscutum*, making it (at the very least) a mesotrophic taxon.
614
615 The transition from nannofossil assemblages with dominant *Neobiscutum* (14 μm^3 average cell
616 volume) to those with higher relative abundances of *Futyania* (322 μm^3 average cell volume) and
617 *Cruciplacolithus* (155-475 μm^3 average cell volume) almost certainly contributed to the 3x increase in
618 wt. % $CaCO_3$ that was also observed at this time (Figure 2d, Alvarez et al., 2019). This would have
619 greatly improved the effectiveness of coccolith calcite as organic matter ballasts (Figure 7b), further
620 enhancing biological pump efficiency. However, as the *Neobiscutum* → *Futyania* transition occurred
621 across an unconformity, it is uncertain whether nannofossil assemblage changes drove enhanced
622 biological pump efficiency or vice versa. For example, a paleoenvironmental factor such as warming
623 may have increased surface ocean stratification and lowered nutrient availability, driving the observed
624 shifts in nannofossil assemblages that in turn led to increased biological pump efficiency. Conversely,
625 a different parameter such as the faster recovery of planktic foraminifera compared to nannoplankton,
626 could have led to enhanced biological pump efficiency, lowering surface ocean nutrient availability and
627 driving the transition from eutrophic-to meso/oligotrophic-adapted nannoplankton communities. This
628 causality conundrum highlights the need for multiproxy records that document changes in nannofossil

and planktic foraminifera assemblages, the planktic to benthic foraminiferal $\delta^{13}C$ gradient and temperature proxy data at a high temporal resolution.

The remainder of the *Futyania* acme is characterized by a gradual decline in *Futyania* relative to *Cruciplacolithus* (Figure 2a). *Coccolithus* became an important component of assemblages beginning at ca. 63.86 Ma, and gradually increased in relative abundance throughout the *Futyania* acme, whilst *Praeprinsius* maintained a consistently low (~10%) relative abundance until ~62.63 Ma. The increased proportion of pelagic taxa such as *Cruciplacolithus* and *Coccolithus* with quasi-stability in the geochemical data, suggests a gradual transition to more oligotrophic surface waters between 63.86 and 62.63 Ma, which may have been predominantly ecologically – rather than environmentally – driven (Figures 2-4). At ~62.63 Ma the relative abundance of *Praeprinsius* rapidly increased to comprise >50% of assemblages. For the subsequent ca. 200 kyr, there was significant ecological jostling between *Futyania* and *Praeprinsius*, with the base of the *Praeprinsius* acme tentatively placed at ~62.46 Ma, when assemblages stabilized and *Praeprinsius* maintained its dominance. This 200 kyr transitional interval coincides with a transient ~2.5 % decrease in bulk carbonate $\delta^{18}O$ (Figure 2b), a gradual 1.5 % increase in bulk carbonate $\delta^{13}C$ (Figure 2b), a transient ~0.75 % decrease in bulk organic $\delta^{13}C$ (Figure 2c) and wildly fluctuating wt. % $CaCO_3$ values (Figure 2d). Aside from the bulk carbonate $\delta^{13}C$, these geochemical trends are similar to those during the earlier Dan-C2 event. We therefore speculate that at least some of the paleoecological instability observed in nannofossil assemblages was a result of a further hyperthermal such as the Late Danian Event (LDE), although our current age model indicates that the potential warming event at El Kef occurred earlier (~62.52 Ma) than the estimated age of the LDE (~62.15 Ma; Harbich et al., 2024).

4.1.4 Stage 4 – *The Praeprinsius* acme (~62.35 to 62.46 Ma): The youngest ~100 kyr of the El Kef record is characterized by the high dominance of *Praeprinsius* (generally >70%) with very low relative abundances of *Cruciplacolithus* and *Coccolithus*, especially compared to the *Futyania* acme. The decline in oligotrophic-adapted taxa and the dominance of *Praeprinsius* – a presumed opportunistic, eutrophic-adapted taxon (Jiang et al., 2019) suggests a reversion to higher nutrient surface waters. The part of the *Praeprinsius* acme recorded at El Kef, is associated with only minor changes in the geochemical proxy records suggesting relatively quiescent paleoenvironmental conditions. Overall, the persistence of high dominance, low diversity nannoplankton acmes for at least 3.65 Myr post-impact, suggests that ecosystem function was restored a lot slower at El Kef than at ODP Site 1209, where the acme regime ended within ~1.8 Myr (Alvarez et al., 2019).

4.2 Regional vs. bathymetric controls on post K/Pg nannoplankton community composition

The two-way cluster analysis indicates that El Kef has an exceptionally dominant *Neobiscutum* and *Futyania* acme compared to other Tethyan sites (Clusters 2 and 3B; Figure 5), most of which sample slightly deeper (~600 to 1500 m) paleo-water depths. Curiously, the Egyptian continental shelf sites Wadi Hamama and Gebel Qreiya – which are estimated to be shallower (100-200 m; Tantawy, 2003) than El Kef (200-600 m; Alegret et al., 2022) – also do not have a well-defined *Neobiscutum* or *Futyania* acme, and are instead characterized by the distinctive 'disaster' assemblages observed at all of the analyzed upper/mid bathyal Tethyan sites (Cluster 1; Figure 5). Examination of the Northern Hemisphere NMDS results indicates that this is unusual, as the dominance of certain nannoplankton taxa is primarily driven by paleobathymetry (Figure 6b) rather than regional controls on assemblages (Figure 6a). For example, earliest Danian disaster assemblages (calcispheres, *Braarudosphaera* and

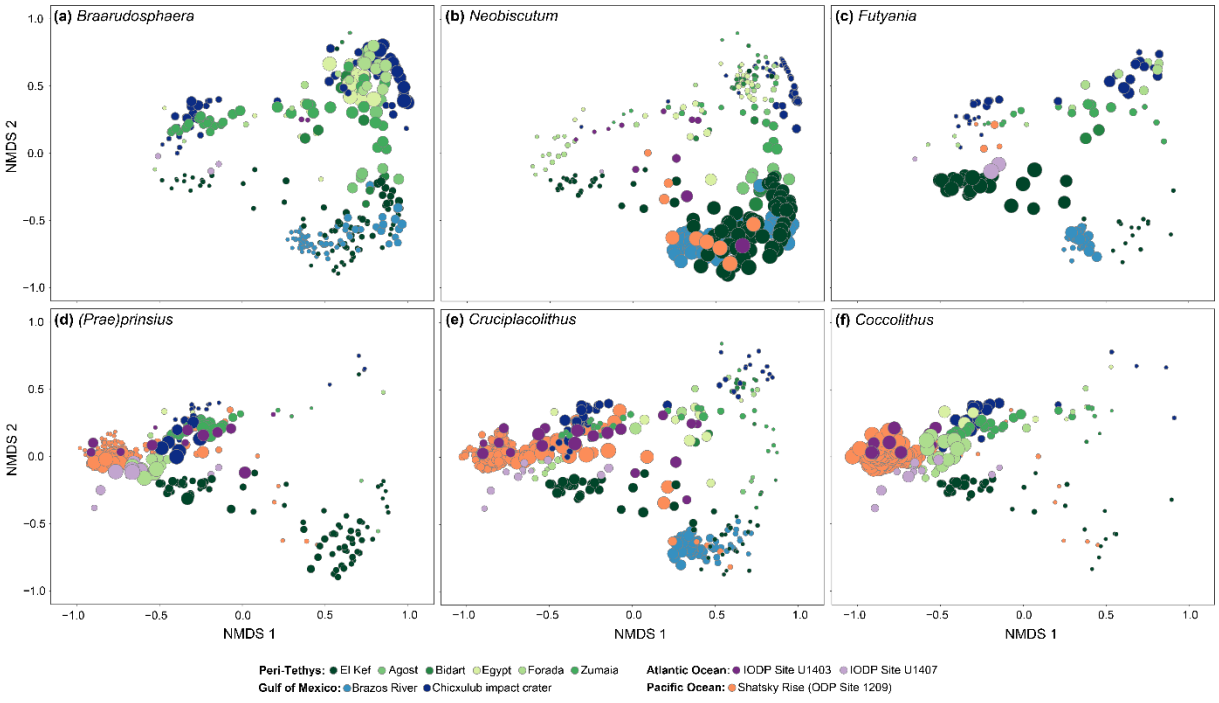

674

Figure 8. Nonmetric multidimensional scaling (NMDS) ordination plots showing sample scores coded by site. The size of each point (sample score) is scaled by the relative abundance of the six major acme-forming taxa: (a) *Braarudosphaera*, (b) *Neobiscutum,* (c) *Futyania,* (d) *(Prae)prinsius*, (e) *Cruciplacolithus,* (f) *Coccolithus*.

675 Cretaceous survivors such as *Cyclagelosphaera*) were a common feature of continental slope and
676 bathyal sites (Figure 6b) regardless of ocean basin (Figure 6a), whereas a true, long-lasting
677 *Neobiscutum* acme was confined to only El Kef (a shelf-slope site) and Brazos River (a continental shelf
678 site in the Gulf of Mexico). The high dominance of *Neobiscutum* at both other shelf/slope sites thus
679 makes it even more unusual that this acme was not observed in the Eygptian outcrop sections.
680
681 To explore this further, we scaled the NMDS scores in Figure 6 by the relative abundance of the six
682 acme-forming nannofossil taxa (*Braarudosphaera*, *Neobiscutum*, *Futyania*, *Praeprinsius*,
683 *Cruciplacolithus* and *Coccolithus*) within that sample, coded by both ocean basin/region (Figure 8) and
684 estimated paleo-water depth (Figure 9). A comparison of these two figures confirms that with the
685 exception of *Braarudosphaera* and *Praeprinsius*, the geographic distribution of the acme-forming
686 nannofossil taxa is predominantly driven by paleobathymetry (Figure 9). Although *Braarudosphaera* is
687 more abundant in the Tethys Ocean and the Gulf of Mexico (Figure 8a), its acme is restricted to
688 continental slope-to-middle bathyal paleoenvironments (~600 to 1500 m paleo-water depth), with the
689 exception of the previously-identified shallow Egyptian sections (Figure 9a). In contrast, as
690 aforementioned, *Neobiscutum* only formed a sustained long-term acme at outer shelf/upper slope
691 sites (~100-600 m paleo-water depth; Figure 9b), with bathyal sites such as ODP Site 1209 and IODP
692 Site U1403 only comprising dominant *Neobiscutum* within a limited number of samples (Figures 8b;
693 9b). The lower than expected relative abundance of *Neobiscutum* at Wadi Hamama and Gebel Qreiya,
694 may therefore either be a function of the unique position of these outcrop sections in the eastern
695 Tethys and/or their slightly more tropical paleolatitude compared to the other Tethyan sites (Figure
696 1). Although Tethyan ocean circulation patterns are poorly constrained for the late Cretaceous/early
697 Paleocene, neodymium isotopic records (Soudry et al., 2006) indicate that the strength of the
698 westward flowing Tethyan Circumglobal Current may have increased during the latest Cretaceous due

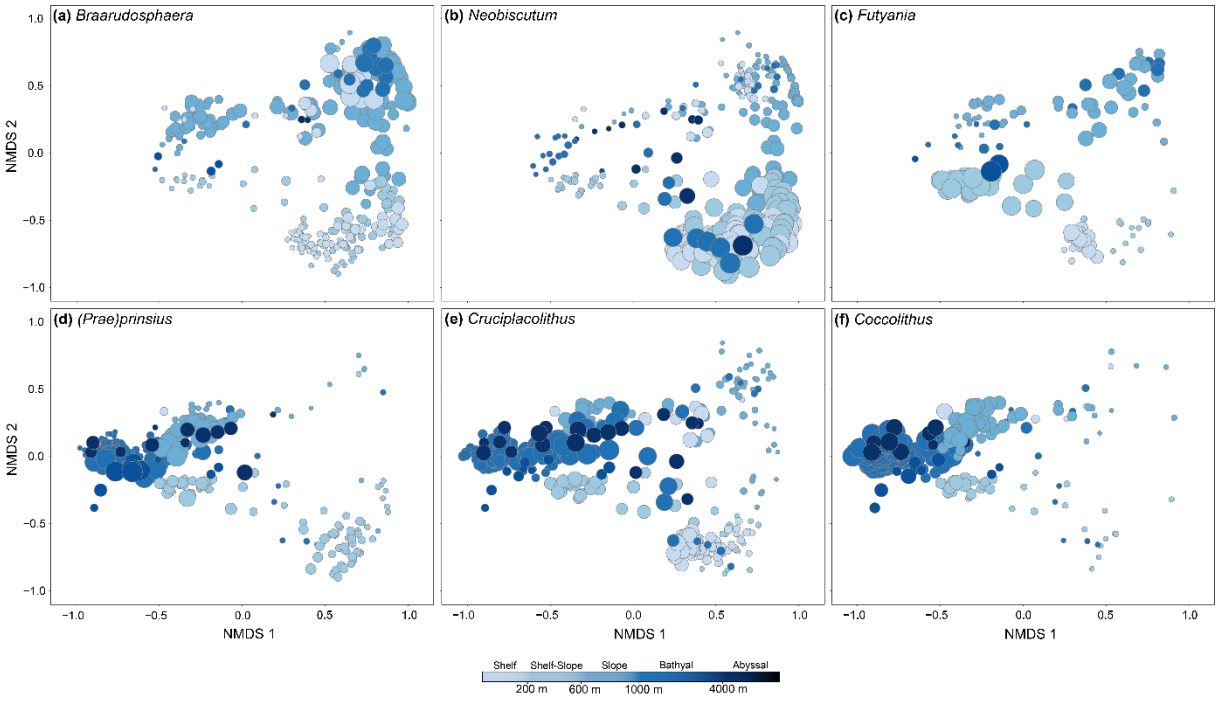

699

Figure 9. Nonmetric multidimensional scaling (NMDS) ordination plots showing sample scores coded by palebathymetry. The size of each point (sample score) is scaled by the relative abundance of the six major acme-forming taxa: (a) *Braarudosphaera*, (b) *Neobiscutum,* (c) *Futyania,* (d) *(Prae)prinsius*, (e) *Cruciplacolithus,* (f) *Coccolithus*.

700 to the opening of the equatorial Atlantic gateway at the Cenomanian-Turonian boundary (Poulsen et
701 al., 2003) and or/an enhanced latitudinal temperature gradient following Santonian cooling (Barrera
702 & Savin, 1999). The latter mechanism would have strengthened the trade winds, leading to increased
703 incursion of Pacific waters into the eastern Tethys and enhanced upwelling along the southeastern
704 Tethyan continental shelf (Soudry et al., 2006), potentially explaining the observed differences in the
705 Egyptian nannofossil assemblages compared to the other (western) Tethyan sites. Alternatively, the
706 low-paleolatitude (~10 °N) location of Wadi Hamama and Gebel Qrieya combined with a potentially
707 enhanced latitudinal temperature gradient, may have driven the formation of a *Braarudosphaera*
708 acme due to hyperstratification: the same mechanism invoked for the *Braarudosphaera* spike during
709 the Dan-C2 event at El Kef. Although we consider the second explanation more plausible, nannofossil
710 records from the mid-latitude eastern Tethys are required to support this hypothesis.
711
712 In comparison to all other acme-forming taxa*, Futyania* is observed at much lower overall relative
713 abundances across all sites and only forms a true acme (>40% of assemblages) at El Kef (Figures 8; 9).
714 This taxon was observed to some extent in all of the examined ocean basins, but appears to have been
715 particularly well-adapted to outer-shelf/upper slope surface ocean environments (200-600 m paleo-
716 water depth; Figure 9c), with Brazos River being the only other site where *Futyania* reached a
717 sufficiently high abundance to be almost considered an acme (Figure 8c). Conversely, the *Praeprinsius*
718 acme is a common feature of almost all sites included in the NMDS analysis during the later recovery
719 interval (Figure 8d) regardless of paleo-water depth (Figure 9d). It is important to note that the
720 seemingly higher abundance of *Praeprinsius* at bathyal and abyssal sites is because only samples up to
721 the first ~3.5 Myr of the Danian were included in this analysis (with the exception of the Brazos River
722 record, which only extends to 2.5 Myr post-impact), to ensure that a similar time interval was being
723 compared across all sites. However, as the *Praeprinsius* acme was not fully established until later than

this at El Kef – and likely also at other shelf/slope sites – it is not visible in our Northern Hemisphere NMDS analysis.

The long-ranging Paleocene taxon *Cruciplacolithus* is present at all of the examined sites, but only forms its own acme at bathyal ODP Site 1209 (Figure 8e). At all other sites, *Cruciplacolithus* is a secondary component of one of the other acmes, such as the *Neobiscutum* acme at Brazos River, the *Futyania* acme at El Kef, and the *Praeprinsius* and/or *Coccolithus* acme at bathyal/abyssal sites in the Gulf of Mexico, peri-Tethys and North Atlantic Ocean (Figure 8e). Therefore, whilst *Cruciplacolithus* likely had a paleoecological preference for bathyal (potentially oligotrophic) environments (Jiang et al., 2010), it seems to have had a fairly broad range of environmental tolerances and a relatively cosmopolitan distribution during the early Danian. This is especially true when compared to *Coccolithus* (Figures 8f, 9f), which only forms a major acme at bathyal sites within the analyzed ~3.5 Myr post-impact interval. Overall, when considered together, it appears as though paleobathymetry was the major driver in the abundance patterns of acme-forming nannofossil taxa during the K/Pg recovery interval, with a possible secondary regional control for *Braarudosphaera*.

4.3 Geographic heterogeneity in nannoplankton acme successions and implications for the restoration of biological pump efficiency

4.3.1 Patterns in nannoplankton acme successions: Although the NMDS results provide a general overview of geographic differences in early Danian nannofossil assemblages, they cannot be used to compare the durations of each acme and the timings of the switchovers between them. Therefore, in order to look at this in more detail, we produced cumulative abundance plots of the major acme-forming taxa for the eight sites with sufficiently high age control (Figure 10). In addition to El Kef, this included Forada (Fornaciari et al., 2007), Brazos River (Schueth, 2009) and Chicxulub (Jones et al., 2019) – with ages estimated based on linear sedimentation rates between biostratigraphic tie points – and Zumaia (Jiang et al., 2019), ODP Site 1209 (Alvarez et al., 2019) and IODP Sites U1403 and U1407 (Bown et al., 2023), which have their own published age models. Due to temporal limitations at some of the sites, we focused our comparison on a ~63.79 - 66.02 Ma stratigraphic interval.

The resulting plots provide further support that early Danian nannoplankton community composition was primarily a function of paleobathymetry, with sites sharing similar oceanic settings having the exact same sequence of nannoplankton acmes regardless of location (Figure 10). As revealed by the NMDS analysis, shallow continental shelf/slope sites have a particularly prominent *Neobiscutum* acme, which persists for the entire duration of the 2.2 Myr record at Brazos River (Figure 10e) and likely for a similar length of time at El Kef once the unconformity is taken into account (Figure 10a). The biggest difference between the Brazos River and El Kef records is the abundance of *Cruciplacolithus*, which begins to increase much earlier at Brazos River (~65.4 Ma) compared to at El Kef (~64.1 Ma). In contrast, the El Kef record includes ancestral *Praeprinsius* cf. *vegrandis* specimens – which were not recognized at Brazos River – and a clearly defined *Futyania* acme. However, as the Brazos River record does not extend beyond >2.2 Myr post-impact, it is possible that the apparent absence of the *Futyania* acme here is simply a function of data limitation. The *Praeprinsius* acme is similarly not observed in this restricted stratigraphic record as it occurred ~3.5 Myr after the mass extinction at El Kef. Overall, the currently available data indicates that the succession of nannoplankton acmes in shallow marine settings was *Neobiscutum* → *Futyania* → *Praeprinisius*, with the acme regime persisting well beyond

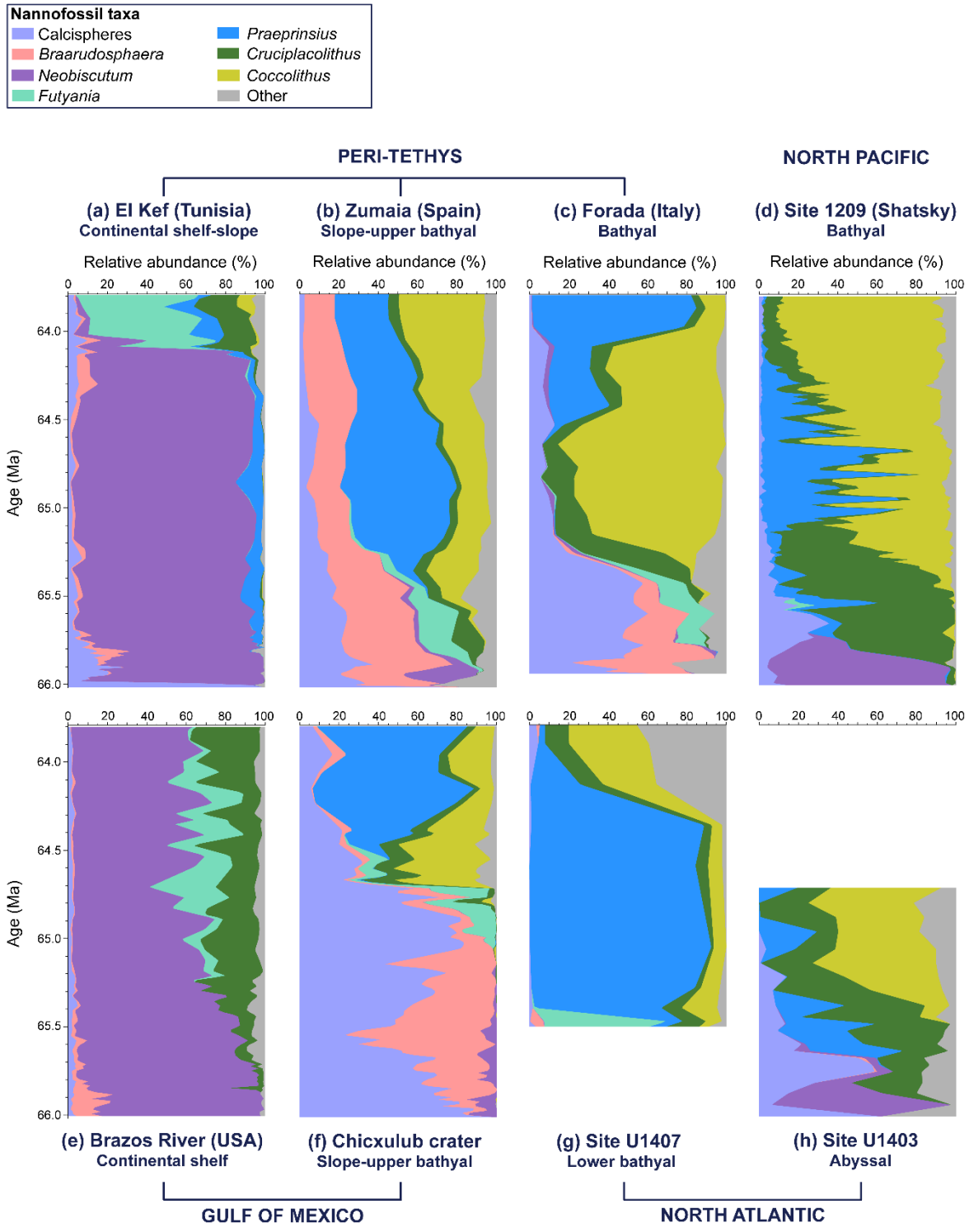

Figure 10. Cumulative frequency plots showing the relative abundance of the six major acme-forming nannofossil taxa (and calcispheres) between ~63.8 and 66.0 Ma at eight Northern Hemisphere sites. (a) Nannofossil relative abundances at El Kef, Tunisia (this study). (b) Nannofossil relative abundances at Zumaia, Spain (Jiang et al. 2019). (c) Nannofossil relative abundances at Forada, Italy (Fornaciari et al. 2007). (d) Nannofossil relative abundances at ODP Site 1209: Shatsky Rise, North Pacific Ocean (Alvarez et al. 2019). (e) Nannofossil relative abundances at Brazos River, USA (Schueth 2009). (f) Nannofossil relative abundances at IODP-ICDP Site M0077A: Chicxulub impact crater, Gulf of Mexico (Jones et al. 2019). (g) Nannofossil relative abundances at IODP Site U1407, North Atlantic Ocean (Bown et al. 2023). (h) Nannofossil relative abundances at IODP Site U1403, North Atlantic Ocean (Bown et al. 2023).

2.2 Myr post-impact. However, additional shelf/slope records are required to confirm these recovery patterns.

Nannofossil assemblages at the upper bathyal sites Zumaia (peri-Tethys) and Chicxulub (Gulf of Mexico) also share very similar acme characteristics (Figure 10b; f), with the calcisphere/*Braarudosphaera*/Cretaceous survivor acme being the dominant feature of the earliest Danian recovery. *Neobiscutum* is also present – albeit at much lower abundances than at shallower sites – and *Futyania* is a similarly minor component of assemblages during the latter part of this acme. The 'disaster' acme at both upper bathyal sites is succeeded by the increased abundance of *Cruciplacolithus* and – most importantly – *Coccolithus*, which is rare in contemporaneous shelf-slope assemblages. In the Chicxulub impact crater, *Coccolithus* even formed a short-lived (~250 kyr), weakly defined acme before being replaced by *Praeprinsius*. Although present in both upper bathyal records, the *Praeprinsius* acme at Chicxulub occurred ~1 Myr later than at Zumaia, likely reflecting more severe, unstable environmental conditions at ground zero (Jones et al., 2019). Nevertheless, even at Chicxulub, this acme occurred ~2 Myr earlier than at El Kef, suggesting faster nannoplankton recovery in these slightly deeper marine environments. The acme regime remained active until the end of both upper bathyal records (~2.2 Myr post-impact), indicating that full ecological recovery had not yet occurred. Overall, the acme succession in lower slope – upper bathyal settings appears to have followed the sequence: Cretaceous survivor acme → *Coccolithus* (pseudo)acme → *Praeprinsius* acme.

The two examined middle bathyal records – Forada, Italy in the peri-Tethys (Figure 10c) and ODP Site 1209 (Shatsky Rise) in the equatorial North Pacific (Figure 10d) – exhibit notably different recovery patterns. Forada most closely resembles upper bathyal sites, particularly Zumaia, for the first ~1 Myr of the Danian, as both are characterized by a survivor (rather than *Neobiscutum*) acme (Figure 10b, c, d). *Futyania* also formed a pseudo-acme ~250 kyr post-impact at both Forada (Figure 10c) and Zumaia (Figure 10b), but was very rare at Shatsky Rise (Figure 10d). In contrast, the ODP Site 1209 record is characterized by a *Neobiscutum* acme immediately following the mass extinction (Figure 10d). This acme lasted for ~250 kyr years before being replaced by the *Cruciplacolithus* acme, which was also coincident with a small spike in calcispheres (but not *Braarudosphaera*; Figure 10d). The *Coccolithus* acme developed at a similar time (700 kyr post-impact) at Forada and Shatsky Rise. However, at Shatsky Rise, the *Coccolithus* acme was interrupted by the *Praeprinsius* acme, which ended ~1.8 Myr post-impact and is interpreted as the first major milestone in nannoplankton recovery (Alvarez et al., 2019). In contrast, the *Praeprinsius* acme did not occur until 64.5 Ma at Forada and persisted until the top of the record (~63.8 Ma), closely mirroring the recovery pattern observed at Chicxulub (Figure 10f). The distinct acme successions observed at these two middle bathyal sites likely reflects differences in ocean connectivity and circulation between the peri-Tethys (Forada) and the Pacific Ocean (Shatsky Rise), with the peri-Tethys representing a relatively restricted shallow sea receiving 'older' westward-flowing Pacific water via the Tethyan Circumglobal Current (Soudry et al., 2006). For this reason, we suggest two separate acme sequences for middle bathyal environments: *Neobiscutum* → *Cruciplacolithus* → *Coccolithus* → *Praeprinsius* for fully open-ocean settings such as Shatsky Rise, and Cretaceous survivor acme → *Futyania* pseudo-acme → *Coccolithus* → *Praeprinsius* for more restricted oceanic settings in the peri-Tethys.

Although the first ~500 kyr of the Danian are missing from lower bathyal IODP Site U1407 in the North Atlantic (Bown et al., 2023; Fig. 10g), nannoplankton recovery patterns closely resemble those at Chicxulub (Fig. 10f), with the notable exception of a very prominent *Praeprinsius* acme that began much earlier (~65.4 Ma) than at any other bathyal site. The subsequent termination of the acme

regime and transition to stable assemblages comprising of long-ranging Paleocene taxa (e.g., *Towieus*), occurred almost synchronously at Site U1407 and Shatsky Rise, confirming that nannoplankton communities recovered more rapidly in open-ocean than in shallower marine environments. In contrast, abyssal Site U1403 (also in the North Atlantic) preserves only the first ~1.25 Myr of the Danian (Bown et al., 2023; Fig. 10h). Overall, the nannoplankton recovery patterns at this site closely resemble those at Shatsky Rise, indicating relative homogeneity between the North Atlantic and North Pacific during the earliest Danian.

4.3.2 Implications for the restoration of biological pump efficiency: The causal relationship between nannoplankton recovery and the restoration of biological pump efficiency is still open to debate, due to the various complex mechanisms that connect these two processes. For example, it unknown whether: (Option 1) increased nannoplankton cell volume during the early Danian enhanced the ballasting of organic matter, which drove higher biological pump efficiency, (Option 2) another mechanism independent of nannoplankton recovery drove the restoration of biological pump efficiency, leading to lower nutrient surface waters that favored the proliferation of nannoplankton taxa with larger cell volumes, or (Option 3) nannoplankton recovery and the restoration of biological pump efficiency were completely decoupled. Our El Kef data provides tentative support that nannoplankton recovery and biological pump efficiency were linked – especially between the *Neobiscutum* → *Futyania* acme transition – discounting Option 3. However, it is not possible with our current data to determine whether nannoplankton recovery led (Option 1) or lagged (Option 2) the restoration of biological pump efficiency. In contrast, records from ODP Site 1209 suggest a decoupling between nannoplankton recovery and biological pump efficiency during the acme regime (i.e., the first ~1.8 Myr of the Danian), although it should be noted that the ODP Site 1209 nannoplankton data were compared to the $\delta^{13}C$ gradient at ODP Site 1262 (Walvis Ridge), which were characterized by very different nannofossil assemblages (Jiang et al., 2010; Schueth et al., 2015) and export productivity patterns (Hull & Norris, 2011). Therefore, future studies should focus on comparing nannofossil abundances and geochemical reconstructions of biological pump efficiency at the same site using highly-resolved age models.

If increased nannoplankton cell volume did drive enhanced biological pump efficiency (Option 1), the distinct acme successions in shallower vs. deeper oceanic settings may at least partially explain the global heterogeneity in export productivity (Hull & Norris, 2011). For example, at shallow marine sites, the very small cell volumes that characterized the *Neobiscutum* acme (14 μm^3; Alvarez et al., 2019) dominated assemblages for at least 1.8 Myr post-impact (Figure 10), with contemporaneous bathyal sites already consisting of more diverse nannofossil assemblages with an average cell volume of ~300 μm^3 (Alvarez et al., 2019). This large disconnect between assemblage-level average cell volumes suggests – especially if Option 1 is the case – that the restoration of biological pump efficiency occurred slower-to-faster along a continental shelf-to-open ocean transect. However, as relatively rare taxa with larger cell volumes disproportionately contribute to carbonate production, this hypothesis needs to be more rigorously tested via the application of nannofossil biogeochemical trait models, which can be used to estimate changes in community-level calcite production through time (Gibbs et al., 2018; Sheward et al., 2024). The stratigraphically-expanded El Kef cores are ideal for this purpose as they contain the common coccospheres (complete nannoplankton cell coverings) required for these analyses, including intermediate morphotypes that offer the exciting opportunity to explore how biogeochemical traits evolved within a single species. Combining such abundance-weighted

nannofossil biogeochemical trait data with planktic-benthic $\delta^{13}C$ records will help resolve the causal relationship between nannoplankton recovery and the restoration of biological pump efficiency during the early Danian.

5. Conclusions

Our new El Kef nannofossil dataset – sampling an outer shelf/upper slope setting in the peri-Tethys Ocean – suggests that the nannoplankton acme regime persisted for at least 3.65 Myr after the K/Pg mass extinction event: ~1.85 Myr longer than in the pelagic Pacific Ocean. The exact sequence of nannoplankton acmes was predominantly driven by paleobathymetry (i.e., the position of a site along a continental shelf-to-open ocean transect) at both a regional (Tethyan) and global scale, whilst the timing of the switchovers between acmes had at least some regional control. We speculate that the differences in nannoplankton acme sequences between oceanic settings could have directly influenced the restoration of biological pump efficiency. Specifically, the earlier establishment of nannoplankton communities with a higher average cell volume (and likely enhanced ballasting potential) at open-ocean vs. continental shelf sites may have led to the faster restoration of biological pump efficiency in deeper marine environments. In the future, this should be tested directly by combining estimates for nannofossil carbonate production with reconstructions of biological pump efficiency at the same site, helping to resolve the causal relationship between these two mechanisms following the most recent mass extinction event in Earth history.

Acknowledgements

The authors would like to thank Shijun Jiang and Gilen Bernaola for providing nannofossil data from Bidart and Zumaia for our global analysis and to Heather Birch, Michael Henehan, Ursula Röhl, Johan Vellekoop and Jessica Whiteside for providing feedback on a much earlier version of this manuscript. Research funding was provided by a NASA Exobiology grant (# here) awarded to T.B….

Conflict of interest

The authors declare no conflicts of interest relevant to this study.

Data Availability Statement

The new calcareous nannofossil relative abundance data and updated age model tables are available from PANGAEA (doi here).

References

Alegret, L., Arreguín-Rodríguez, G.J. & Thomas, E. (2022). Oceanic productivity after the Cretaceous/Paleogene impact: Where do we stand? The view from the deep. In C. Koeberl, P. Claeys & A. Montanari (Eds.) *From the Guajira Desert to the Apennines, and from Mediterranean Microplates to the Mexican Killer Asteroid: Honoring the Career of Walter Alvarez: Geological Society of America Special Paper 557* (pp. 449–470). https://doi.org/10.1130/2022.2557(21)

Alegret, L., & Thomas, E. (2009). Food supply to the seafloor in the Pacific Ocean after the Cretaceous/Paleogene boundary event. *Marine Micropaleontology, 73(1-2),* 105-116. https://doi.org/10.1016/j.marmicro.2009.07.005

Alegret, L., & Thomas, E. (2013). Benthic foraminifera across the Cretaceous/Paleogene boundary in the Southern Ocean (ODP Site 690): Diversity, food and carbonate saturation. *Marine Micropaleontology, 105,* 40-51. https://doi.org/10.1016/j.marmicro.2013.10.003

Alegret, L., Thomas, E. & Lohmann, K.C. (2012). End-Cretaceous marine mass extinction not caused by productivity collapse. *Proceedings of the National Academy of Sciences*, *109(3)*, 728-732. https://doi.org/10.1073/pnas.1110601109

Alvarez, L.W., Alvarez, W., Asaro, F. & Michel, H.V. (1980). Extraterrestrial cause for the Cretaceous-Tertiary extinction. *Science*, *208(4448)*, 1095-1108. https://doi.org/10.1126/science.208.4448.1095

Alvarez, S.A., Gibbs, S.J., Bown, P.R., Kim, H., Sheward, R.M. & Ridgwell, A. (2019). Diversity decoupled from ecosystem function and resilience during mass extinction recovery. *Nature*, *574*, 242-245. https://doi.org/10.1038/s41586-019-1590-8

Arreguín-Rodríguez, G. J., Barnet, J. S., Leng, M. J., Littler, K., Kroon, D., Schmidt, D. N. et al. (2021). Benthic foraminiferal turnover across the Dan-C2 event in the eastern South Atlantic Ocean (ODP Site 1262). *Palaeogeography, Palaeoclimatology, Palaeoecology, 572,* 110410. https://doi.org/10.1016/j.palaeo.2021.110410

Artemieva, N., Morgan, J., & Expedition 364 Science Party. (2017). Quantifying the release of climate-active gases by large meteorite impacts with a case study of Chicxulub. *Geophysical Research Letters, 44(20),* 10-180,188. https://doi.org/10.1002/2017GL074879

Barnet, J. S., Littler, K., Westerhold, T., Kroon, D., Leng, M. J., Bailey, I. et al. (2019). A high-fidelity benthic stable isotope record of late Cretaceous–early Eocene climate change and carbon-cycling. *Paleoceanography and Paleoclimatology, 34(4),* 672-691. https://doi.org/10.1029/2019PA003556

Barrera, E., & Savin, S. M. (1999). Evolution of late Campanian-Maastrichtian marine climates and oceans. In E. Barrera & C.C. Johnson (Eds.), *Evolution of the Cretaceous Ocean–Climate System: Geological Society of America Special Paper 332*, (pp. 245-282). https://doi.org/10.1130/0-8137-2332-9.245

Birch, H.S., Coxall, H.K., Pearson, P.N., Kroon, D. & Schmidt, D.N. (2016). Partial collapse of the marine carbon pump after the Cretaceous-Paleogene boundary. *Geology*, *44 (4)*, 287-290. https://doi.org/10.1130/G37581.1

Birch, H., Schmidt, D. N., Coxall, H. K., Kroon, D., & Ridgwell, A. (2021). Ecosystem function after the K/Pg extinction: decoupling of marine carbon pump and diversity. *Proceedings of the Royal Society B, 288(1953),* 20210863. https://doi.org/10.1098/rspb.2021.0863

Bown, P. (2005). Selective calcareous nannoplankton survivorship at the Cretaceous-Tertiary boundary. *Geology*, *33(8)*, 653-656. https://doi.org/10.1130/G21566AR.1

Bown, P. R., Kim, H., & Gibbs, S. J. (2023). Danian calcareous nannofossil evolution and taxonomy with focus on sites from the North Atlantic Ocean (IODP Expedition 342, Sites U1403 and U1407). *Journal of Nannoplankton Research, 41(2),* 110-157. https://doi.org/10.58998/jnr3943

Bown, P.R., Lees, J.A. & Young, J.R. (2004). Calcareous nannoplankton evolution and diversity through time. In H.R. Thierstein & J.R. Young (Eds.) *Coccolithophores* (pp. 481-508). Berlin, Heidelberg: Springer. https://doi.org/10.1007/978-3-662-06278-4_18

Bown, P.R. & Young, J.R. (1998) Techniques. In P.R. Bown (Ed.), *Calcareous nannofossil biostratigraphy* (pp. 16-28)*.* London: Chapman and Hall.

Bralower, T. J., Cosmidis, J., Heaney, P. J., Kump, L. R., Morgan, J. V., Harper, D. T. et al. (2020). Origin of a global carbonate layer deposited in the aftermath of the Cretaceous-Paleogene boundary impact. *Earth and Planetary Science Letters, 548,* 116476. https://doi.org/10.1016/j.epsl.2020.116476

Brugger, J., Feulner, G., Hofmann, M., & Petri, S. (2021). A pronounced spike in ocean productivity triggered by the Chicxulub impact. *Geophysical Research Letters, 48(12),* e2020GL092260. https://doi.org/10.1029/2020GL092260

Chiarenza, A. A., Farnsworth, A., Mannion, P. D., Lunt, D. J., Valdes, P. J., Morgan, J. V., & Allison, P. A. (2020). Asteroid impact, not volcanism, caused the end-Cretaceous dinosaur extinction. *Proceedings of the National Academy of Sciences, 117(29)*, 17084-17093. https://doi.org/10.1073/pnas.2006087117

Coccioni, R., Frontalini, F., Bancalà, G., Fornaciari, E., Jovane, L., & Sprovieri, M. (2010). The Dan-C2 hyperthermal event at Gubbio (Italy): Global implications, environmental effects, and cause (s). *Earth and Planetary Science Letters, 297(1-2),* 298-305. https://doi.org/10.1016/j.epsl.2010.06.031

Coxall, H.K., D'Hondt, S. & Zachos, J.C. (2006). Pelagic evolution and environmental recovery after the Cretaceous-Paleogene mass extinction. *Geology*, *34(4)*, 297-300. https://doi.org/10.1130/G21702.1

Culver, S. J. (2003). Benthic foraminifera across the Cretaceous–Tertiary (K–T) boundary: a review. *Marine Micropaleontology, 47(3-4),* 177-226. https://doi.org/10.1016/S0377-8398(02)00117-2

D'Hondt, S., Donaghay, P., Zachos, J.C., Luttenberg, D. & Lindinger, M. (1998). Organic carbon fluxes and ecological recovery from the Cretaceous-Tertiary mass extinction. *Science*, *282(5387)*, 276-279. https://doi.org/10.1126/science.282.5387.276

Esmeray-Senlet, S., Wright, J. D., Olsson, R. K., Miller, K. G., Browning, J. V., & Quan, T. M. (2015). Evidence for reduced export productivity following the Cretaceous/Paleogene mass extinction. *Paleoceanography, 30(6),* 718-738. https://doi.org/10.1002/2014PA002724

Fornaciari, E., Giusberti, L., Luciani, V., Tateo, F., Agnini, C., Backman, J. et al. (2007). An expanded Cretaceous− Tertiary transition in a pelagic setting of the Southern Alps (central-western Tethys). *Palaeogeography, Palaeoclimatology, Palaeoecology*, *255(1-2)*, 98-131. https://doi.org/10.1016/j.palaeo.2007.02.044

Fraass, A.J., Kelly, D.C. & Peters, S.E. (2015). Macroevolutionary history of the planktic foraminifera. *Annual Review of Earth and Planetary Sciences*, *43*, 139-166. https://doi.org/10.1146/annurev-earth-060614-105059

Gibbs, S.J., Sheward, R.M., Bown, P.R., Poulton, A.J. & Alvarez, S.A. (2018). Warm plankton soup and red herrings: calcareous nannoplankton cellular communities and the Palaeocene–Eocene Thermal Maximum. *Philosophical Transactions of the Royal Society A: Mathematical, Physical and Engineering Sciences*, *376(2130),* 20170075. https://doi.org/10.1098/rsta.2017.0075.

Hagino, K., Takano, Y., & Horiguchi, T. (2009). Pseudo-cryptic speciation in *Braarudosphaera bigelowii* (Gran and Braarud) Deflandre. *Marine Micropaleontology, 72(3-4),* 210-221. https://doi.org/10.1016/j.marmicro.2009.06.001

Harbich, M., Barnet, J. S., Rae, J. W., & Kroon, D. (2024). Warming, acidification, and calcification feedback during the first hyperthermal of the Cenozoic—The Latest Danian Event. *Geology, 52(1),* 51-55. https://doi.org/10.1130/G51330.1

Harrell Jr, F.E. (2025). Hmisc: Harrell Miscellaneous. https://CRAN.R-project.org/package=Hmisc

Henehan, M.J., Ridgwell, A., Thomas, E., Zhang, S., Alegret, L., Schmidt, D.N. et al. (2019). Rapid ocean acidification and protracted Earth system recovery followed the end-Cretaceous Chicxulub

impact. *Proceedings of the National Academy of Sciences*, *116(45)*, 22500-22504. https://doi.org/10.1073/pnas.1905989116

Hsü, K. J., & Mckenzie, J. A. (1985). A "Strangelove" ocean in the earliest Tertiary. In E.T. Sundquist & W.S. Broecker (Eds.), *The Carbon Cycle and Atmospheric CO_2: Natural Variations Archean to Present. Geophysical Monographs Series 32,* 487-492. https://doi.org/10.1029/GM032p0487

Hull, P.M., Bornemann, A., Penman, D.E., Henehan, M.J., Norris, R.D., Wilson, P.A. et al. (2020). On impact and volcanism across the Cretaceous-Paleogene boundary. *Science*, *367(6475)*, 266-272. https://doi.org/10.1126/science.aay5055

Hull, P.M. & Norris, R.D. (2011). Diverse patterns of ocean export productivity change across the Cretaceous-Paleogene boundary: New insights from biogenic barium. *Paleoceanography*, *26*, PA3205. https://doi.org/10.1029/2010PA002082

Jiang, S., Bralower, T.J., Patzkowsky, M.E., Kump, L.R. & Schueth, J.D. (2010). Geographic controls on nannoplankton extinction across the Cretaceous/Palaeogene boundary. *Nature Geoscience*, *3*, 280-285. https://doi.org/10.1038/ngeo775

Jiang, S., Chen, X., & Bernaola, G. (2019). Environmental controls on calcareous nannoplankton response to the Cretaceous/Paleogene mass extinction in the Tethys realm. *Palaeogeography, Palaeoclimatology, Palaeoecology, 515,* 134-142. https://doi.org/10.1016/j.palaeo.2017.12.044

Jones, H.L., Lowery, C.M. & Bralower, T.J. (2019). Delayed calcareous nannoplankton boom-bust successions in the earliest Paleocene Chicxulub (Mexico) impact crater. *Geology*, *47(8)*, 753-756. https://doi.org/10.1130/G46143.1

Jones, H. L., Westerhold, T., Birch, H., Hull, P., Negra, M. H., Röhl, U. et al. (2023). Stratigraphy of the Cretaceous/Paleogene (K/Pg) boundary at the Global Stratotype Section and Point (GSSP) in El Kef, Tunisia: New insights from the El Kef Coring Project. *GSA Bulletin, 135(9-10),* 2451-2477. https://doi.org/10.1130/B36487.1

Junium, C. K., Zerkle, A. L., Witts, J. D., Ivany, L. C., Yancey, T. E., Liu, C., & Claire, M. W. (2022). Massive perturbations to atmospheric sulfur in the aftermath of the Chicxulub impact. *Proceedings of the National Academy of Sciences, 119(14),* e2119194119. https://doi.org/10.1073/pnas.2119194119

Kolde, R. (2025). pheatmap: Pretty Heatmaps. https://CRAN.R-project.org/package=pheatmap

Knoll, A.H. & Follows, M.J. (2016). A bottom-up perspective on ecosystem change in Mesozoic oceans. *Proceedings of the Royal Society B: Biological Sciences*, *283(1841)*, 20161755. https://doi.org/10.1098/rspb.2016.1755

Lamolda, M. A., Melinte-Dobrinescu, M. C., & Kaiho, K. (2016). Calcareous nannoplankton assemblage changes linked to paleoenvironmental deterioration and recovery across the Cretaceous–Paleogene boundary in the Betic Cordillera (Agost, Spain). *Palaeogeography, Palaeoclimatology, Palaeoecology, 441,* 438-452. https://doi.org/10.1016/j.palaeo.2015.10.003

Liebrand, D., Raffi, I., Fraguas, Á., Laxenaire, R., Bosmans, J.H., Hilgen, F.J. et al. (2018). Orbitally Forced Hyperstratification of the Oligocene South Atlantic Ocean. *Paleoceanography and Paleoclimatology*, *33*, 511-529. https://doi.org/10.1002/2017PA003222

Lowery, C.M., Bown, P.R., Fraass, A.J. & Hull, P.M. (2020). Ecological Response of Plankton to Environmental Change: Thresholds for Extinction. *Annual Review of Earth and Planetary Sciences*, *48*, 403-429. https://doi.org/10.1146/annurev-earth-081619-052818

Lowery, C. M., Jones, H. L., Bralower, T. J., Cruz, L. P., Gebhardt, C., Whalen, M. T. et al. (2021). Early Paleocene paleoceanography and export productivity in the Chicxulub crater. *Paleoceanography and Paleoclimatology, 36(11),* e2021PA004241. https://doi.org/10.1029/2021PA004241

MacLeod, K. G., Huber, B. T., Tabor, C., Mitra, S., Wheatley, R., Harrison, C. et al. (2025). Isotopic evidence from a Brazos River (Texas, USA) Cretaceous/Paleogene boundary section consistent with a pulse of greenhouse warming shortly after the Chicxulub impact. *Global and Planetary Change, 253,* 104924. https://doi.org/10.1016/j.gloplacha.2025.104924

MacRae, R. A., Fensome, R. A., & Williams, G. L. (1996). Fossil dinoflagellate diversity, originations, and extinctions and their significance. *Canadian Journal of Botany, 74(11),* 1687-1694. https://doi.org/10.1139/b96-205

Mai, H., Speijer, R.P. & Schulte, P. (2003). Calcareous index nannofossils (coccoliths) of the lowermost Paleocene originated in the late Maastrichtian. *Micropaleontology*, *49(2)*, 189-195. https://doi.org/10.2113/49.2.189

Mather, B. R., Müller, R. D., Zahirovic, S., Cannon, J., Chin, M., Ilano, L. et al. (2024). Deep time spatio-temporal data analysis using pyGPlates with PlateTectonicTools and GPlately. *Geoscience Data Journal, 11(1),* 3-10. https://doi.org/10.1002/gdj3.185

McLachlan, S. M., & Pospelova, V. (2021). Calcareous dinoflagellate cyst distribution across the K/Pg boundary at DSDP site 577, Shatsky Rise, western North Pacific Ocean. *Marine Micropaleontology, 168,* 102057. https://doi.org/10.1016/j.marmicro.2021.102057

Morgan, J. V., Bralower, T. J., Brugger, J., & Wünnemann, K. (2022). The Chicxulub impact and its environmental consequences. *Nature Reviews Earth & Environment, 3(5),* 338-354. https://doi.org/10.1038/s43017-022-00283-y

Müller, R. D., Flament, N., Cannon, J., Tetley, M. G., Williams, S. E., Cao, X. et al. (2022). A tectonic-rules-based mantle reference frame since 1 billion years ago – implications for supercontinent cycles and plate–mantle system evolution [Data set]. In Solid Earth (1.2.4, Vol. 13, pp. 1127–1159). Zenodo. https://doi.org/10.5281/zenodo.13636799

Oksanen, J., Simpson, G.L., Guillaume Blanchet, F., Kindt, R., Legendre, P., Minchin, P.R. et al. (2025). vegan: Community Ecology Package, version 2.7-2. https://CRAN.R-project.org/package=vegan

Poulsen, C. J., Gendaszek, A. S., & Jacob, R. L. (2003). Did the rifting of the Atlantic Ocean cause the Cretaceous thermal maximum? *Geology, 31(2),* 115-118. https://doi.org/10.1130/0091-7613(2003)031<0115:DTROTA>2.0.CO;2

R Core Team. (2025, December 04). R: A Language and Environment for Statistical Computing (Version 4.5.1) [Software]. R Foundation for Statistical Computing, Vienna, Austria. https://www.R-project.org/.

Renaudie, J., Drews, E. L., & Böhne, S. (2018). The Paleocene record of marine diatoms in deep-sea sediments. *Fossil Record, 21(2),* 183-205. https://doi.org/10.5194/fr-21-183-2018, 2018.

Romein, A. J. T. (1977). Calcareous nannofossils from the Cretaceous/Tertiary boundary interval in the Barranco del Gredero (Caravaca, Prov. Murcia, SE Spain). *Proceedings of the Koninklijke Nederlandse Akademie ven Wetenschappen Amsterdam Ser. B, 80,* 256-279.

Schneider, L. J., Bralower, T. J., Kump, L. R., & Patzkowsky, M. E. (2013). Calcareous nannoplankton ecology and community change across the Paleocene-Eocene Thermal Maximum. *Paleobiology, 39(4),* 628-647. https://doi.org/10.1666/12050

Schueth, J.D. (2009). A Multivariate Analysis of the Recovery of Calcareous Nannoplankton and Planktonic Foraminifera from the Cretaceous/Paleogene (K/P) Mass Extinction. (Master's thesis). Retrieved from (https://etda.libraries.psu.edu/catalog/10281). University Park, PA: Penn State University.

Schueth, J.D., Bralower, T.J., Jiang, S. & Patzkowsky, M.E. (2015). The role of regional survivor incumbency in the evolutionary recovery of calcareous nannoplankton from the Cretaceous/Paleogene (K/Pg) mass extinction. *Paleobiology*, *41(4)*, 661-679. https://doi.org/10.1017/pab.2015.28

Schulte, P., Alegret, L., Arenillas, I., Arz, J.A., Barton, P.J., Bown, P.R. et al. (2010). The Chicxulub asteroid impact and mass extinction at the Cretaceous-Paleogene boundary. *Science*, *327(5970)*, 1214-1218. https://doi.org/10.1126/science.1177265

Senel, C. B., Kaskes, P., Temel, O., Vellekoop, J., Goderis, S., DePalma, R. et al. (2023). Chicxulub impact winter sustained by fine silicate dust. *Nature Geoscience, 16(11),* 1033-1040. https://doi.org/10.1038/s41561-023-01290-4

Sepúlveda, J., Alegret, L., Thomas, E., Haddad, E., Cao, C. & Summons, R.E. (2019). Stable Isotope Constraints on Marine Productivity Across the Cretaceous-Paleogene Mass Extinction. *Paleoceanography and Paleoclimatology*, *34*, 1195-1217. https://doi.org/10.1029/2018PA003442

Sheward, R. M., Herrle, J. O., Fuchs, J., Gibbs, S. J., Bown, P. R., & Eibes, P. M. (2024). Biogeochemical traits of a high latitude South Pacific Ocean calcareous nannoplankton community during the Oligocene. *Paleoceanography and Paleoclimatology, 39(12),* e2024PA004946. https://doi.org/10.1029/2024PA004946

Sims, P. A., Mann, D. G., & Medlin, L. K. (2006). Evolution of the diatoms: insights from fossil, biological and molecular data. *Phycologia, 45(4),* 361-402. https://doi.org/10.2216/05-22.1

Soudry, D., Glenn, C.R., Nathan, Y., Segal, I. & VonderHaar, D. (2006). Evolution of Tethyan phosphogenesis along the northern edges of the Arabian–African shield during the Cretaceous–Eocene as deduced from temporal variations of Ca and Nd isotopes and rates of P accumulation. *Earth-Science Reviews*, *78(1-2),* 27-57. https://doi.org/10.1016/j.earscirev.2006.03.005

Takano, Y., Hagino, K., Tanaka, Y., Horiguchi, T., & Okada, H. (2006). Phylogenetic affinities of an enigmatic nannoplankton, *Braarudosphaera bigelowii* based on the SSU rDNA sequences. *Marine Micropaleontology, 60(2),* 145-156. https://doi.org/10.1016/j.marmicro.2006.04.002

Tantawy, A.A.A.M. (2003). Calcareous nannofossil biostratigraphy and paleoecology of the Cretaceous–Tertiary transition in the central eastern desert of Egypt. *Marine Micropaleontology*, *47(3-4)*, 323-356. https://doi.org/10.1016/S0377-8398(02)00135-4

Thomas, E. (1990). Late Cretaceous-early Eocene mass extinctions in the deep sea. In V.L. Sharpton & P.D. Ward (Eds.), *Global catastrophes in Earth history; An interdisciplinary conference on impacts, volcanism, and mass mortality: Geological Society of America Special Paper 247* (pp. 481-495). https://doi.org/10.1130/SPE247-p481

Vellekoop, J., Sluijs, A., Smit, J., Schouten, S., Weijers, J.W., Damsté, J.S.S. & Brinkhuis, H. (2014). Rapid short-term cooling following the Chicxulub impact at the Cretaceous–Paleogene boundary.

Proceedings of the National Academy of Sciences, *111(21)*, 7537-7541. https://doi.org/10.1073/pnas.1319253111

Vellekoop, J., Smit, J., van de Schootbrugge, B., Weijers, J.W., Galeotti, S., Damste, J.S.S. & Brinkhuis, H. (2015). Palynological evidence for prolonged cooling along the Tunisian continental shelf following the K–Pg boundary impact. *Palaeogeography, Palaeoclimatology, Palaeoecology*, *426,* 216-228. https://doi.org/10.1016/j.palaeo.2015.03.021

Vellekoop, J., Woelders, L., Açikalin, S., Smit, J., Van De Schootbrugge, B., Yilmaz, I.O. et al. (2017). Ecological response to collapse of the biological pump following the mass extinction at the Cretaceous-Paleogene boundary. *Biogeosciences*, *14*, 885-900. https://doi.org/10.5194/bg-14-885-2017

Wade, B. S., Pearson, P. N., Berggren, W. A., & Pälike, H. (2011). Review and revision of Cenozoic tropical planktonic foraminiferal biostratigraphy and calibration to the geomagnetic polarity and astronomical time scale. *Earth-Science Reviews, 104(1-3),* 111-142. https://doi.org/10.1016/j.earscirev.2010.09.003

Wei, T. & Simko, V. (2024). R package 'corrplot': Visualization of a Correlation Matrix (Version 0.95). https://github.com/taiyun/corrplot.

Westerhold, T., Marwan, N., Drury, A. J., Liebrand, D., Agnini, C., Anagnostou, E. et al. (2020). An astronomically dated record of Earth's climate and its predictability over the last 66 million years. *Science, 369(6509),* 1383-1387. https://doi.org/10.1126/science.aba6853

Wickham, H. (2016). ggplot2: Elegant Graphics for Data Analysis. New York: Springer-Verlag. https://ggplot2.tidyverse.org